Ground and low-lying excited states of propadienylidene ($H_2C{=}C{=}C$:) obtained by negative ion photoelectron spectroscopy

John F. Stanton,[1] Etienne Garand,[2] Jongjin Kim,[2] Tara I. Yacovitch,[2] Christian Hock,[2] Amanda S. Case,[3] Elisa M. Miller,[3] Yu-Ju Lu,[3] Kristen M. Vogelhuber,[3] Scott W. Wren,[3] Takatoshi Ichino,[1] John P. Maier,[4] Robert J. McMahon,[5] David L. Osborn,[6] Daniel M. Neumark,[2] and W. Carl Lineberger[3]

[1]*Institute for Theoretical Chemistry, Department of Chemistry and Biochemistry, The University of Texas at Austin, Austin, Texas 78712, USA*
[2]*Department of Chemistry, University of California, Berkeley, California 94720, USA*
[3]*JILA and Department of Chemistry and Biochemistry, University of Colorado, Boulder, Colorado 80309, USA*
[4]*Department of Chemistry, University of Basel, CH-4056 Basel, Switzerland*
[5]*Department of Chemistry, University of Wisconsin, Madison, Wisconsin 53706-1322, USA*
[6]*Combustion Research Facility, Sandia National Laboratories, Livermore, California 94551-0969, USA*

(Received 25 January 2012; accepted 1 March 2012; published online 4 April 2012)

A joint experimental-theoretical study has been carried out on electronic states of propadienylidene (H_2CCC), using results from negative-ion photoelectron spectroscopy. In addition to the previously characterized $\tilde{X}^1A_1$ electronic state, spectroscopic features are observed that belong to five additional states: the low-lying $\tilde{a}^3B_1$ and $\tilde{b}^3A_2$ states, as well as two excited singlets, $\tilde{A}^1A_2$ and $\tilde{B}^1B_1$, and a higher-lying triplet, $\tilde{c}^3A_1$. Term energies (T_0, in cm^{-1}) for the excited states obtained from the data are: 10 354±11 ($\tilde{a}^3B_1$); 11 950±30 ($\tilde{b}^3A_2$); 20 943±11 ($\tilde{c}^3A_1$); and 13 677±11 ($\tilde{A}^1A_2$). Strong vibronic coupling affects the $\tilde{A}^1A_2$ and $\tilde{B}^1B_1$ states as well as $\tilde{a}^3B_1$ and $\tilde{b}^3A_2$ and has profound effects on the spectrum. As a result, only a weak, broadened band is observed in the energy region where the origin of the $\tilde{B}^1B_1$ state is expected. The assignments here are supported by high-level coupled-cluster calculations and spectral simulations based on a vibronic coupling Hamiltonian. A result of astrophysical interest is that the present study supports the idea that a broad absorption band found at 5450 Å by cavity ringdown spectroscopy (and coincident with a diffuse interstellar band) is carried by the $\tilde{B}^1B_1$ state of H_2CCC. © *2012 American Institute of Physics*. [http://dx.doi.org/10.1063/1.3696896]

I. INTRODUCTION

The C_3H_2 isomers constitute a family of reactive organic species that play a role in the chemistry of harsh environments, including combustion,[1,2] planetary atmospheres,[3–5] and interstellar space.[6–8] These extremely hydrogen-deficient species possess unusual bonding arrangements and high reactivity. Singlet cyclopropenylidene (c-C_3H_2) is the global minimum on the potential energy surface, with triplet propynylidene (HCCCH; E_{rel} = 10 kcal/mol) and singlet propadienylidene ($H_2C{=}C{=}C$: or, in a more abbreviated form, H_2CCC, E_{rel} = 13 kcal/mol) at slightly higher energy.[9] Propadienylidene (H_2CCC) was first generated and characterized in an argon matrix by Maier and co-workers.[10,11] Following the laboratory detection of H_2CCC in the gas phase via millimeter-wave spectroscopy,[12] this polar singlet C_3H_2 carbene was soon discovered in two different astronomical sources, TMC-1 and IRC+10 216.[13] Subsequent millimeter-wave and Fourier transform microwave spectroscopy studies yielded rotational constants for the ground state of H_2CCC (Refs. 14 and 15) which, when combined with theoretical calculations, indicated the ground state geometry to be a near prolate top with C_{2v} symmetry.[14,16] McMahon and co-workers measured the electronic absorption spectrum of propadienylidene in argon[17] and neon matrices.[18] Transitions to the three lowest-lying singlet excited states were observed at 1.73, 2.00, and 4.84 eV, with each transition exhibiting substantial vibrational structure. The lowest-energy transition, $\tilde{A}^1A_2 \leftarrow \tilde{X}^1A_1$, is forbidden by symmetry, but becomes weakly allowed through vibronic coupling with the $\tilde{B}^1B_1$ state.[17–19] Vibronic coupling analysis also explains the rich vibrational progression in the $\tilde{B}^1B_1 \leftarrow \tilde{X}^1A_1$ transition.[18,19] Photoexcitation into the $\tilde{B}^1B_1 \leftarrow \tilde{X}^1A_1$ transition of H_2CCC results in equilibration (presumably via a cyclic structure) of the two carbon atoms at the terminal and central positions—a degenerate process that becomes observable through isotopic (^{13}C) labeling.[9,20] This process is an efficient mechanism for internal conversion in propadienylidene, and occurs through a seam of conical intersections between the $\tilde{A}^1A_2$ and $\tilde{B}^1B_1$ states.[19]

The extensive pattern of visible absorption features, in a species that is known to be an interstellar molecule, invites speculation concerning the possibility of singlet propadienylidene as a carrier for some of the diffuse interstellar bands (DIBs).[21] Although the neon matrix spectrum provides the foundation for the electronic spectroscopy of H_2CCC, a high-resolution gas phase spectrum is essential for comparison with the DIBs. Maier and co-workers measured the electronic spectrum of H_2CCC in the gas phase using cavity ringdown spectroscopy (CRDS). They observed levels associated with

the symmetry-forbidden $\tilde{A}^1A_2 \leftarrow \tilde{X}^1A_1$ transition, but were initially unable to observe the stronger, symmetry-allowed $\tilde{B}^1B_1 \leftarrow \tilde{X}^1A_1$ transition because of the short lifetime of the $\tilde{B}^1B_1$ state.[22,23] Subsequently, they succeeded in measuring the prominent vibronic features of the $\tilde{B}^1B_1 \leftarrow \tilde{X}^1A_1$ transition at 4881 and 5450 Å, thus providing the basis for assigning these features in the DIB spectrum to propadienylidene.[24] Additional discussion of this topic is deferred to Sec. V of this paper.

Photoelectron spectroscopy of the propadienylidene anion, H_2CCC^-, provides another means of investigating the electronic states of H_2CCC.[25,26] Unlike conventional absorption spectroscopy, the selection rules in photoelectron spectroscopy offer the opportunity to probe a different group of electronics states (those that can formally be viewed in the molecular orbital picture as being obtained by a single-electron removal from the anion). Propadienylidene anion has a $^2B_1$ ground state with the $[\text{core}](1b_1)^2(7a_1)^2(2b_2)^2(2b_1)^1$ molecular orbital configuration; removal of the unpaired electron gives the $\tilde{X}^1A_1$ electronic state, while removal of an electron from the $(2b_2)$, $(7a_1)$, or $(1b_1)$ orbitals yields the $\tilde{A}^1A_2$, $\tilde{B}^1B_1$, or $\tilde{C}^1A_1$ states, respectively. The triplet states of propadienylidene are accessed along with the singlet states, since photodetachment from the latter three orbitals would also yield the $\tilde{b}^3A_2$, $\tilde{a}^3B_1$, and $\tilde{c}^3A_1$ states, respectively. The earlier photoelectron spectrum of H_2CCC^- showed the origins for both the lowest singlet and triplet states, which exhibit a separation of 1.29 eV.[26] Although the measurements revealed complex spectral features located between the origins of the singlet and triplet manifolds, the photon energy was not high enough to access other excited states of H_2CCC. In this paper, we report the photoelectron spectra of propadienylidene anion using several variants of photoelectron spectroscopy,[27–29] where the excited singlet and triplet states are observed as well. The analysis and interpretation of these spectra rely heavily on computational and theoretical studies involving high level electronic structure calculations and a sophisticated treatment of vibronic coupling.

II. EXPERIMENTAL DETAILS

The experimental photoelectron spectra were collected in three laboratories using three different detection methods: Negative ion photoelectron spectroscopy (NIPES) at JILA, photoelectron velocity-map imaging (VMI) at JILA, and slow electron velocity-map imaging (SEVI) at Berkeley. In the NIPES experiments, greater control over the anion chemistry is afforded by a flowing afterglow ion source; additionally, the energy resolution is constant over the entire spectrum and the peak intensities are virtually free from threshold effects.[30] Higher photon energies are available in the VMI experiments, enabling detection of the highly excited states of neutral species. SEVI is a variant of VMI: it selectively detects slow electrons in order to obtain the highest resolution photoelectron spectra in this work. Because electrons are detached very close to threshold, SEVI can be limited by threshold effects that influence the intensity of the observed peaks.

A. Negative ion photoelectron spectroscopy

The NIPES apparatus, described in Refs. 27, 31, 32, consists of four main sections: an anion source, a mass filter, a laser-anion interaction region, and an electron kinetic energy (eKE) analyzer. Atomic oxygen radical anion, O^-, is formed in a flowing afterglow ion source. Allene reacts with O^- to generate H_2CCC^-: $H_2CCCH_2 + O^- \rightarrow H_2CCC^- + H_2O$.[25,26] Ions are collisionally cooled to approximately 300 K and can be further cooled with a liquid nitrogen jacket to obtain a "cold spectrum" of ions at ~150 K. Anions are then mass-selected via a Wien velocity filter ($m/\Delta m \sim 60$).[33] The mass-selected ion beam (~70 pA) is decelerated and focused into the laser interaction region where the 1-W output from a single-mode, continuous-wave Ar ion laser (363.79 nm, 27 488 cm^{-1}) is built up to about 100 W in an optical cavity. A rotatable half-wave plate varies the polarization of the laser. This allows for control of the angle between the electric-field vector of the laser beam and the photoelectron collection axis.[34] Photoelectrons ejected orthogonal to both the laser and ion beams enter a hemispherical energy analyzer. The photoelectron signal is recorded as a function of eKE using a position-sensitive detector with a resolution of roughly 80 cm^{-1} (FWHM). The absolute kinetic energy scale is calibrated[27,35] before and after each data set using the well-known electron affinity (EA) of atomic oxygen.[36] Spectra are reported in terms of electron binding energy (eBE), defined as the difference between the photon energy, $h\nu$, and eKE: eBE $= h\nu$ - eKE. When peaks in a photoelectron spectrum do not overlap, absolute eBEs are determined with an accuracy of ~40 cm^{-1}.

B. Photoelectron velocity-map imaging

The VMI apparatus, described previously,[28] consists of a pulsed ion source,[37,38] a Wiley-McLaren time-of-flight mass spectrometer (TOF-MS),[39] a ns-pulsed, tunable-laser system, and a VMI (Refs. 40 and 41) photoelectron spectrometer. H_2CCC^- is formed via H_2^+ abstraction from allene by O^- (Refs. 25, 26, 42, and 43) in a pulsed supersonic entrainment reactor.[44] The reactor comprises a central and two side pulsed valves (0.8-mm orifice) operating at a repetition rate of 80 Hz with individual timings and pulse widths. The middle valve provides the main expansion using 1% allene seeded in Ar at a backing pressure of 50 psig. One of the adjacent valves entrains neat N_2O (99%, Scott specialty gases) at a backing pressure of 2 psig into the allene gas expansion. A guided, collinear beam of 1-keV electrons, emitted from a continuous electron gun, collides with the gas expansion to produce slow secondary electrons. The interaction of slow secondary electrons with N_2O yields the O^- reactant by dissociative electron attachment. The O^- anion subsequently reacts with allene to produce H_2CCC^-.

The anions are perpendicularly extracted and mass-separated via the Wiley-McLaren TOF-MS. The mass-selected propadienylidene anions are photodetached by temporally overlapping the ion beam with a linearly polarized laser pulse (parallel to the detector face) ranging from 245 to 325 nm. The tunable light is produced by frequency doubling

the signal output of a 355-nm pumped optical parametric oscillator. Subsequently, the VMI photoelectron spectrometer, which is in the direction perpendicular to both the anion and laser beams, acquires the kinetic energy distribution of the photodetached electrons. The calibration of the energy scale for the VMI spectra is performed using the known transitions of O^- and I^-.[36,45–47] These spectra typically extend over a 0–8000 cm^{-1} eKE range, with a corresponding 80–400 cm^{-1} energy resolution. When peaks in a spectrum do not overlap, the uncertainty in the absolute eBE is again approximately the HWHM of the peak.

C. Slow electron velocity-map imaging

The SEVI apparatus has been described in detail in Refs. 29 and 48. SEVI is a high-resolution variant of photoelectron spectroscopy in which mass-selected anions are photodetached at a series of wavelengths. The resulting photoelectrons are collected by VMI (Ref. 41) using relatively low extraction voltages, with the goal of selectively detecting slow electrons over a narrow range of eKEs.

In this experiment, propadienylidene anion is produced from a gas mixture comprising 1% propene in a balance of argon. The gas mixture, at a stagnation pressure of 300 psi, was expanded into the source vacuum chamber through an Even-Lavie pulsed valve[49] equipped with a grid discharge described in detail in Ref. 50. Anions formed in the gas expansion were perpendicularly extracted into a Wiley-McLaren TOF-MS (Ref. 39) and directed to the detachment region by a series of electrostatic lenses and pinholes. Anions were photodetached between the repeller and the extraction plates of the VMI stack using the gently focused frequency-doubled output of a Nd:YAG-pumped dye laser. The photoelectron cloud formed was then coaxially extracted down a 50-cm flight tube and mapped onto a detector. The detector comprises a pair of time-gated, imaging-quality microchannel plates coupled to a phosphor screen.[40] Events on the screen were collected by a charge-coupled device camera and sent to a computer. The images were summed, quadrant-symmetrized, smoothed, and inverse-Abel transformed.[51] Photoelectron spectra were obtained via angular integration of the transformed images.

The apparatus is calibrated by acquiring SEVI images of S^- and Cl^- at several different photon energies. With the 350 V VMI repeller voltage used in this study, the Gaussian width (2σ) of the chloride peaks are 4.2 cm^{-1} at 31 cm^{-1} eKE and 28 cm^{-1} at 916 cm^{-1} eKE. Linewidths in the SEVI spectra ($\sim$15 cm^{-1}) are limited by unresolved rotational structure. Since the origin of an unresolved rotational profile may not be aligned with the observed peak maximum, we report error bars of one Gaussian standard deviation (σ) in the SEVI spectra.

III. COMPUTATIONAL ASPECTS

The photoelectron spectrum of H_2CCC^- was analyzed using the vibronic coupling model popularized by Köppel, Domcke, and Cederbaum (KDC).[52] In the present application, the neutral states of H_2CCC are treated by the model Hamiltonian

$$H_{KDC} = T_{KDC} + V_{KDC}, \tag{1}$$

where the kinetic energy matrix (which is assumed diagonal in the (quasi) diabatic representation of electronic states) is given by

$$T_{KDC} = T_N \mathbf{1}, \tag{2}$$

where T_N is the nuclear kinetic energy operator. The potential energy, which is the key element of this model, is given here by the six-state matrix

$$V_{KDC} = \begin{bmatrix} V_{XX} & 0 & 0 & 0 & 0 & 0 \\ 0 & V_{AA} & V_{AB} & 0 & 0 & 0 \\ 0 & V_{AB} & V_{BB} & 0 & 0 & 0 \\ 0 & 0 & 0 & V_{aa} & V_{ab} & 0 \\ 0 & 0 & 0 & V_{ab} & V_{bb} & 0 \\ 0 & 0 & 0 & 0 & 0 & V_{cc} \end{bmatrix}, \tag{3}$$

where the shorthand notations X, A, B, a, b, and c represent the $\tilde{X}^1A_1$, $\tilde{A}^1A_2$, $\tilde{B}^1B_1$, $\tilde{a}^3B_1$, $\tilde{b}^3A_2$, and $\tilde{c}^3A_1$ (diabatic) electronic states of the molecule. Singlet–triplet mixing via spin-orbit coupling is excluded from consideration, as is indicated by the block-diagonal structure of the potential matrix. Moreover, while vibronic coupling between the electronic states with A_2 and B_1 symmetry is important in both the singlet and the triplet, the A_1 states of both spin types have been treated as isolated states, in which the KDC model becomes equivalent to the Franck-Condon treatment.

Each of the diagonal blocks of V_{KDC} is given by a polynomial expansion in terms of the normal coordinates of the anion (which are given explicitly in Table I), viz,

$$V_{II} = V_0^I + \sum_i F_i^{II} q_i + \frac{1}{2}\sum_{ij} F_{ij}^{II} q_i q_j + \frac{1}{6}\sum_{ijk} F_{ijk}^{II} q_i q_j q_k + \frac{1}{24}\sum_{ijkl} F_{ijkl}^{II} q_i q_j q_k q_l. \tag{4}$$

In the above, V_0^I is the (vertical) energy difference between the anion at its equilibrium geometry and the electronic state I. All of the summations are restricted in the sense that each contribution is nonvanishing only if it contains a totally symmetric product of normal coordinates. Consistent with our earlier work on the formyloxyl radical[53]—as well as a recent study of the electronic absorption spectrum of H_2CCC (Ref. 19)—the cubic and quartic force constants above are limited to those which contain only totally symmetric coordinates q_1 through q_4.

Similarly, the interstate coupling blocks in the Hamiltonian are also given by polynomial expansions, except that the non-vanishing terms now have overall b_2 symmetry since this is the direct product of the states (A_2 and B_1 for both triplet and singlet cases) that are coupled by the vibronic interaction. In terms of the normal coordinates of the anion, coordinates q_8 and q_9 are most important in the coupling; both these and their geometric dependence with respect to coordinates q_2 through q_4 were considered in the form of the coupling that

TABLE I. Cartesian coordinates (in bohr) of the $\tilde{X}^2B_1$ state of the propadienylidene anion, along with Cartesian representations (unit length) of the totally symmetric reduced normal coordinates. The approximate descriptions (and positive phase conventions) for the normal coordinates, which can be inferred from the data below, are: q_1 C_1H symmetric stretch (compression); q_2 C_2C_3 stretch (compression); q_3 HC_1H scissor (closing); q_4 C_1C_2 stretch (expansion). The atomic numbering follows Fig. 2.

			Anion coordinates			
C_3			0.00000000	0.00000000	2.66904945	
C_2			0.00000000	0.00000000	0.25683558	
C_1			0.00000000	0.00000000	−2.34874091	
H			−1.74399683	0.00000000	−3.43597801	
H			1.74399683	0.00000000	−3.43597801	
		Normal coordinate q_1			Normal coordinate q_2	
C_3	0.00000000	0.00000000	0.00023263	0.00000000	0.00000000	−0.04073684
C_2	0.00000000	0.00000000	0.00032403	0.00000000	0.00000000	0.05823449
C_1	0.00000000	0.00000000	−0.01202830	0.00000000	0.00000000	−0.01678042
H	0.11764521	0.00000000	0.06829538	−0.00821062	0.00000000	−0.00426996
H	−0.11764521	0.00000000	0.06829538	0.00821062	0.00000000	−0.00426996
		Normal coordinate q_3			Normal coordinate q_4	
C_3	0.00000000	0.00000000	−0.01000344	0.00000000	0.00000000	0.05818837
C_2	0.00000000	0.00000000	0.00296460	0.00000000	0.00000000	0.02143420
C_1	0.00000000	0.00000000	0.03221118	0.00000000	0.00000000	−0.06404715
H	0.10667334	0.00000000	−0.14986139	0.01380848	0.00000000	−0.09272692
H	−0.10667334	0.00000000	−0.14986139	−0.01380848	0.00000000	−0.09272691

was used

$$V_{IJ} = \sum_{i=8}^{9} \lambda_i^{IJ} q_i + \sum_{i=2}^{4}\sum_{j=8}^{9} \lambda_{ij}^{IJ} q_i q_j + \frac{1}{2}\lambda_{229}^{IJ} q_2^2 q_9 + \lambda_{249}^{IJ} q_2 q_4 q_9, \quad (5)$$

the last two terms of which were needed to represent accurately the geometric dependence of the interstate coupling constant λ_9 in both spin states.

The parameters, which are documented completely in Tables II and III, were calculated using high-level coupled-cluster theory in conjunction with an atomic natural orbital basis set,[54] hereafter termed ANO1. For all states, the diagonal blocks of the KDC Hamiltonian were parametrized according to the "adiabatic" parametrization approach described in Refs. 55 and 56. At the minimum-energy C_{2v} structures for all states,[57] quadratic and limited sets of cubic and quartic force constants were calculated by a mixed procedure; the quadratic constants were evaluated by finite difference of analytic first derivatives, while the cubic and quartic constants involving the totally symmetric coordinates were extracted from a fit of a $9 \times 9 \times 9$ grid of energies calculated at points displaced along the active coordinates, q_2, q_3, and q_4. These force constants were calculated in the normal coordinate representation of the anion. In order to transform these potentials to the proper origin of the coordinate system (the anion geometry), Eqs. (12)–(15) of Ref. 56 were used. These latter values—those that are reckoned with respect to the coordinate origin—are listed in Tables II and III. The vertical energy separations were determined at the same level of theory, which give the V_0^I parameters.

For the ground singlet state and the three triplet electronic states, the CCSD(T) treatment of electron correlation[58] was employed; for the two excited singlet states, the very high-level equation of motion[59] technique known as EOMEE-CCSDT (Ref. 60) was used. The equilibrium geometries, harmonic force fields, displacements from the

TABLE II. Linear and quadratic parameters (in cm^{-1}) for quasidiabatic Hamiltonian, expressed in the reduced normal coordinate representation of the $\tilde{X}^2B_1$ state of the propadienylidene anion. See Eqs. (4) and (5) for definitions of all parameters.

	$\tilde{X}^1A_1$	$\tilde{A}^1A_2$	$\tilde{B}^1B_1$	$\tilde{a}^3B_1$	$\tilde{b}^3A_2$	$\tilde{c}^3A_1$
V_0	0	14701	18274	11325	13310	22115
F_2	1221	1318	−2378	−934	1574	−467
F_3	71	479	311	171	466	774
F_4	699	−254	271	823	−39	−1480
F_{22}	2109	1861	1813	1597	1811	2281
F_{23}	−4	55	−19	16	61	8
F_{24}	28	−98	44	−59	−136	141
F_{33}	1500	1359	1474	1465	1336	1542
F_{34}	25	12	23	28	14	1
F_{44}	1017	1007	1065	1030	984	1185
F_{55}	1883	676	471	884	666	623
F_{56}	−210	−46	35	−100	−45	179
F_{66}	140	330	503	436	365	491
F_{88}	1063	863	1141	1021	790	1045
F_{89}	2	182	211	21	260	−84
F_{99}	235	540	707	214[a]	500	240
λ_8	...	604		535		...
λ_9	...	1061		749		...
λ_{28}	...	−80		−73		...
λ_{38}	...	−44		−37		...
λ_{48}	...	−1		8		...
λ_{29}	...	−191		−170		...
λ_{39}	...	−1		−9		...
λ_{49}	...	6		26		...

[a]Empirically adjusted to 314 cm^{-1} in simulated spectra.

TABLE III. Cubic and quartic parameters (in cm^{-1}) for the quasidiabatic Hamiltonian, expressed in the reduced normal coordinate representation of the $\tilde{X}^2B_1$ state of the propadienylidene anion. See Eqs. (4) and (5) for definitions of the various parameters.

	$\tilde{X}^1A_1$	$\tilde{A}^1A_2$	$\tilde{B}^1B_1$	$\tilde{a}^3B_1$	$\tilde{b}^3A_2$	$\tilde{c}^3A_1$
F_{222}	395	451	448	389	460	283
F_{223}	105	95	89	93	97	102
F_{224}	− 318	− 291	− 262	− 297	− 293	− 319
F_{233}	− 17	3	− 9	− 10	7	− 22
F_{234}	25	22	21	24	25	21
F_{244}	− 97	− 81	− 77	− 90	− 83	− 97
F_{333}	130	50	108	107	45	120
F_{334}	− 15	− 1	− 17	− 16	2	− 21
F_{344}	69	72	71	74	73	66
F_{444}	− 224	− 213	− 181	− 224	− 213	− 228
F_{2222}	150	180	162	240	205	160
F_{2223}	4	2	18	9	− 3	11
F_{2224}	− 10	3	− 54	− 12	19	− 33
F_{2233}	2	3	1	3	5	3
F_{2234}	− 19	− 17	− 15	− 19	− 20	− 11
F_{2244}	55	52	42	58	59	37
F_{2333}	− 1	− 1	− 3	− 3	− 1	− 7
F_{2334}	1	0	0	− 1	2	0
F_{2344}	− 14	− 12	− 7	− 11	− 14	− 6
F_{2444}	40	35	19	33	41	19
F_{3333}	40	22	50	47	20	50
F_{3334}	2	7	3	3	6	3
F_{3344}	5	3	3	4	4	3
F_{3444}	− 19	− 18	− 13	− 17	− 20	− 11
F_{4444}	54	48	37	47	52	32
λ_{229}		− 19		− 23		
λ_{249}		17		15		

anion geometry, and various energetic information are given in Table IV (Ref. 61) for all states.

The interstate coupling parameters were calculated at the CCSD level of theory with a slightly smaller contraction of the atomic natural orbital basis set. While the ANO1 basis uses a 4*s*3*p*2*d*1*f* (for C)/4*s*2*p*1*d* (for H) contraction scheme, the basis employed for the interstate coupling calculations (termed ANO0) uses a 3*s*2*p*1*d* on carbon and 2*s*1*p* on hydrogen. These λ_i values were determined analytically using the quasidiabatic coupled-cluster ansatz developed by Ichino *et al.*;[62] these were subsequently differentiated numerically to yield the nonlinear coupling parameters found in Tables II and III. The coupling parameters were determined "vertically"; that is, the values of λ_8 and λ_9 given in Table II are the exact values determined at the *anion geometry*, and the nonlinear parameters come from differentiating these values in this region. Nevertheless, the values of λ_8 and λ_9 calculated directly at the final state geometries differ only negligibly from those calculated from the corresponding polynomial representation (Eq. (5)) that is centered about the coordinate origin (the equilibrium geometry of the anion).

While the adiabatic force constants from the high-level calculations are exactly the same as the diabatic constants in the KDC Hamiltonian for any set of indices that does not include q_8 and q_9, the quadratic constants F_{88}, F_{89}, and F_{99} were determined from the formally exact relation

$$F_{ij}^I = f_{ij}^I - \frac{2\lambda_i^{IJ}\lambda_j^{IJ}}{E_I - E_J}, \tag{6}$$

where F and f are the diabatic and adiabatic constants, respectively, and the energies and coupling constants involving states I and J are those at the minimum energy C_{2v} geometry of state I, as given by the model Hamiltonian. To follow this procedure ensures that the adiabatic potential obtained by diagonalizing the KDC Hamiltonian will be faithful to the actual *ab initio* data in the sense that the adiabatic force constants involving the coupling modes will be coincident with the *ab initio* potential. Overall, the procedure guarantees that the harmonic force fields of the final (neutral) states associated with adiabatic states of the model Hamiltonian are precisely identical to those given by the *ab initio* calculation at the corresponding minimum energy C_{2v} geometries, as are the cubic and quartic constants involving the symmetric modes. The procedure for Hamiltonian parametrization used here is essentially identical to that used in two previous studies in which both good quantitative ($\sim$50 cm^{-1} or better in level positions) and qualitative agreement was achieved between experimental and theoretical spectra.[53,56]

Once constructed, the model Hamiltonian was diagonalized using Lanczos recursions.[63] The spectra shown here included thirty basis functions for modes q_2, q_3, and q_4 in all cases. For simulations of the $\tilde{X}^1A_1$ and $\tilde{c}^3A_1$ states, in which vibronic coupling was not included, ten functions for modes q_5 and q_6 were used in the former and no nonsymmetric modes in the latter state. For calculations on the coupled $\tilde{A}^1A_2$ and $\tilde{B}^1B_1$ spectrum, as well as that featuring $\tilde{a}^3B_1$ and $\tilde{b}^3A_2$, ten functions were used for the coupling modes q_8 and q_9. Two thousand Lanczos recursions were carried out in all cases, which is sufficient to converge the spectra to the point where additional improvements are not discernable in the visual representation of the spectrum.

For the $\tilde{X}^1A_1$ state of propadienylidene, the spectrum of which is free of any interference from excited states, the anharmonic vibrational frequencies were calculated with second-order vibrational perturbation theory (VPT2) (Ref. 64) at the CCSD(T) level with the ANO1 basis set. These calculations are based on an established procedure,[65,66] whereby analytic second derivatives of the energy are numerically differentiated to yield the cubic and quartic constants required by VPT2.[65,66]

Finally, residual deficiencies in the quantum chemical treatment of the various electronic states under study were examined at a yet higher level of theory; the coupled-cluster singles, doubles, triples, and quadruples approximation (CCSDTQ). With the smaller atomic natural orbital basis (ANO0), both CCSDT and CCSDTQ calculations were carried out for the ground singlet and the various triplet states (the latter with an unrestricted Hartree-Fock reference) at their respective equilibrium geometries. Similarly, for the excited singlets, where a single determinant approach is not appropriate, the EOM-CCSDTQ method was employed. Differences in excitation energies (T_e) obtained from the CCSDT and CCSDTQ calculations were taken as a measure of the error in the theoretical values

TABLE IV. Parameters associated with adiabatic potential energy surfaces of H_2CCC. All values for the singlet states are obtained with the CCSDT treatment of electron correlation, with EOMEE-CCSDT used for the excited states. For triplet states and the anion, the CCSD(T) treatment of correlation is used. The ANO1 basis set and the frozen-core approximation were adopted in all calculations. Bond lengths in Ångstroms, angles in degrees; harmonic frequencies and energies are in cm^{-1}. Normal coordinates are in dimensionless units.

			Anion	$\tilde{X}^1A_1$	$\tilde{A}^1A_2$	$\tilde{B}^1B_1$	$\tilde{a}^3B_1$	$\tilde{b}^3A_2$	$\tilde{c}^3A_1$
$r(C_2C_3)$			1.2765	1.2944	1.3255	1.2166	1.2384	1.3312	1.2986
$r(C_1C_2)$			1.3788	1.3330	1.3644	1.4218	1.3681	1.3472	1.4641
$r(C_1H)$			1.0875	1.0859	1.0840	1.0795	1.0808	1.0831	1.0801
$\theta(C_2C_1H)$			121.94	121.30	120.46	119.91	120.37	120.36	119.86
q_1			0	0.00524	0.04186	0.10420	0.07383	0.04913	0.12160
q_2			0	−0.54481	−0.79573	1.12519	0.47893	−0.98452	0.20577
q_3			0	−0.06327	−0.34448	−0.24015	−0.12329	−0.34140	−0.55708
q_4			0	−0.55643	0.25693	−0.13444	−0.71086	0.04157	1.49665
ω_1	a_1	C_1H sym. str.	3084	3123	3129	3176	3167	3147	3166
ω_2		C_2C_3 str.[a]	1877	1997	1656	2151	1956	1637	1864
ω_3		HC_1H scissor	1469	1486	1403	1453	1464	1389	1459
ω_4		C_1C_2 str.[a]	1065	1113	1027	1014	1096	1047	938
ω_5	b_1	HC_1H oop wag	546	1019	610	512	700	605	615
ω_6		$C_1C_2C_3$ oop bend	397	214	359	442	408	378	397
ω_7	b_2	C_1H asym. str.	3145	3210	3226	3285	3268	3243	3286
ω_8		HC_1H ip rock	1035	1048	865	821	985	616	1034
ω_9		$C_1C_2C_3$ ip bend	317	273	175	*886i*	209	*1136i*	269
E_{stab}[b]			...	−449	−611	−1481	−552	−819	−1297
T_e			...	0	14090	16792	10773	12491	20818
T_e[c]			...	0	13955	16358	10872	12612	20944
E_{vert}[d]			...	449	14701	18274	11325	13310	22115

[a]See Reference 70.
[b]Energy at minimum, relative to that at anion geometry.
[c]Includes correction for quadruple excitations, see text.
[d]Energies at anion geometry, relative to neutral ground state minimum.

obtained without quadruples, but with the larger ANO1 basis. The corresponding excitation energies are listed in Table IV, along with the uncorrected values.[67] In addition, Table IV documents details of the calculated structure of all states involved here, as well as their normal mode descriptions and frequencies.

All *ab initio* calculations were done with the CFOUR program system;[68] the MRCC module,[69] as interfaced to CFOUR, was used for the CCSDTQ calculations. Simulations were done with the XSIM package, which will be a part of the next public release of CFOUR.

IV. RESULTS AND DISCUSSION

A. Overview

Before going into details regarding assignment of the spectra obtained in this work, the wide range of energies surveyed makes an overview of our findings useful. Figure 1 shows a composite of VMI, NIPES, and SEVI spectra over the range of eBEs from 12 000 to 38 000 cm^{-1} (1.49–4.71 eV). At the lower end, detachment produces the ground $\tilde{X}^1A_1$ state of propadienylidene, which has a pronounced and easily assignable vibrational progression that extends out to ~20 000 cm^{-1}.

It should be remembered that the ground state electron configuration of H_2CCC^- is

$$[\text{core}](1b_1)^2(7a_1)^2(2b_2)^2(2b_1)^1$$

with the relevant orbitals pictorially displayed in Fig. 2. Note that the singly-occupied $2b_1$ orbital has a π bonding interaction between the two outer carbons (C_2 and C_3) and a π antibonding interaction between the two inner carbons (C_1 and C_2). Thus, detachment from this orbital leads to formation of the $\tilde{X}^1A_1$ state of the neutral, where the outer and inner CC distances become longer and shorter, respectively, than those in the anion. The normal modes associated with these motions, q_2 and q_4,[70] are then expected to be strongly active in the spectrum; this is the explanation for the long vibrational progression seen in the low energy region of Fig. 1. The other photodetachment processes involving the frontier orbitals are those associated with removal of α or β electrons to produce singlet or triplet states, respectively, with A_2, B_1, and A_1 symmetry, in the approximate order of eBEs (see Fig. 3). By Hund's rule, the triplet states will lie lower in energy than the corresponding singlets. The region of the composite spectrum just above 24 000 cm^{-1} is associated with the $\tilde{a}^3B_1$ and $\tilde{b}^3A_2$ triplet states, but the nature of the vibrational progressions is less clear-cut than for the $\tilde{X}^1A_1$ state. It will become clear later that the reason for this can largely be attributed to vibronic coupling between these two low-lying triplets. Inspection of the $7a_1$ and $2b_2$ orbitals that are depopulated in the process leading to these states suggests that the $\tilde{a}^3B_1$ state will have two modestly shorter CC bonds than in the anion and that the $\tilde{b}^3A_2$ state will have a significant change along the q_2 coordinate.[70] Both of these expectations are met in the quantum-chemical calculations (see Tables I and IV),

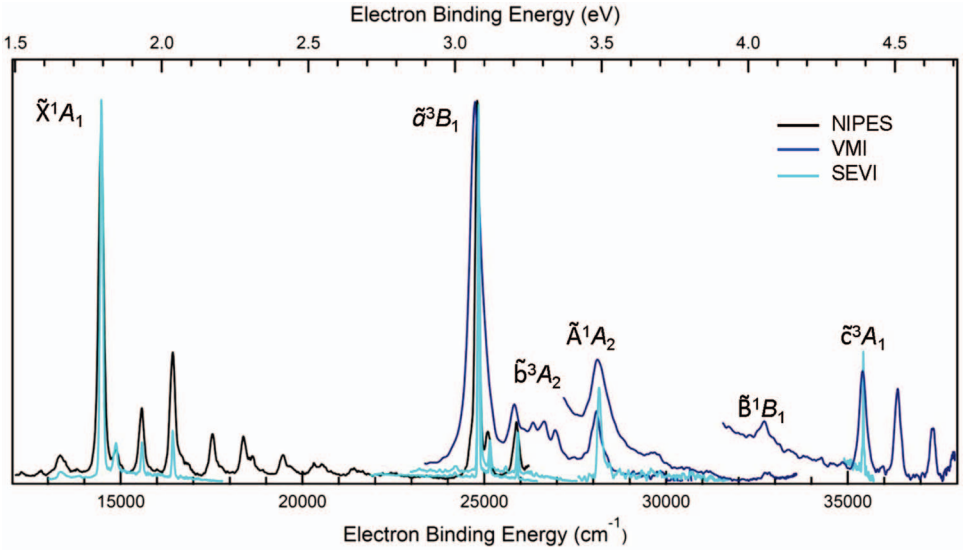

FIG. 1. Composite NIPES, VMI, and SEVI spectra over the range of energies studied in this work. The color scheme, which is used throughout this paper, is: NIPES in black, VMI in dark blue, and SEVI in cyan. The $\tilde{B}^1B_1$ state label does not denote the origin transition for this state.

but without a vivid fingerprint in the nature of the rather complicated spectra.

Above the coupled pair of triplets is the corresponding coupled pair of singlets. It has been known for some time that the energy ordering of the singlet states is $\tilde{A}^1A_2 < \tilde{B}^1B_1$.[17,18,22,23,71] Electronic spectroscopy and quantum-chemical calculations have been successful in understanding the nature of the optical spectrum in the relevant region in terms of a $\tilde{B}^1B_1 \leftarrow \tilde{X}^1A_1$ dipole-allowed transition which is perturbed by a lower-lying (and optically dark) $\tilde{A}^1A_2 \leftarrow \tilde{X}^1A_1$ process. Analysis given in detail later shows that the $\tilde{A}^1A_2$ origin is the prominent feature seen in the composite

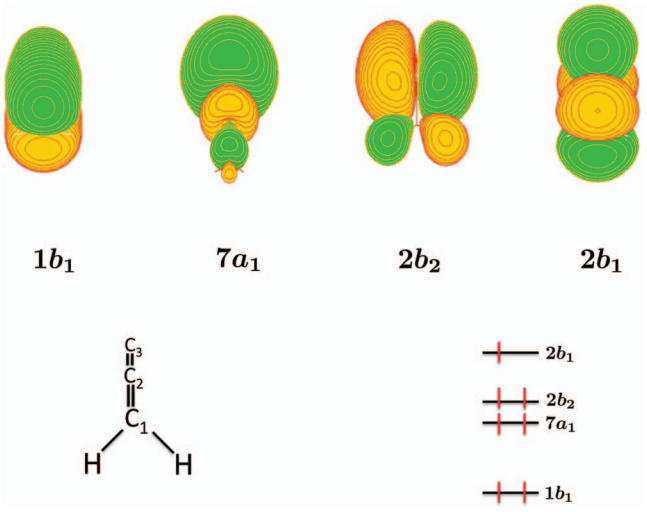

FIG. 2. Frontier molecular orbitals of propadienylidene anion. These calculations used the ANO1 basis (see text) and were carried out using restricted open-shell Hartree-Fock theory at the anion geometry. The view is from 45° above the molecular plane, with the methylene group closest and the linear CCC framework extending away from the eye, and is shown schematically in the lower left-hand side of the figure. The electron configuration shown is that for the anion.

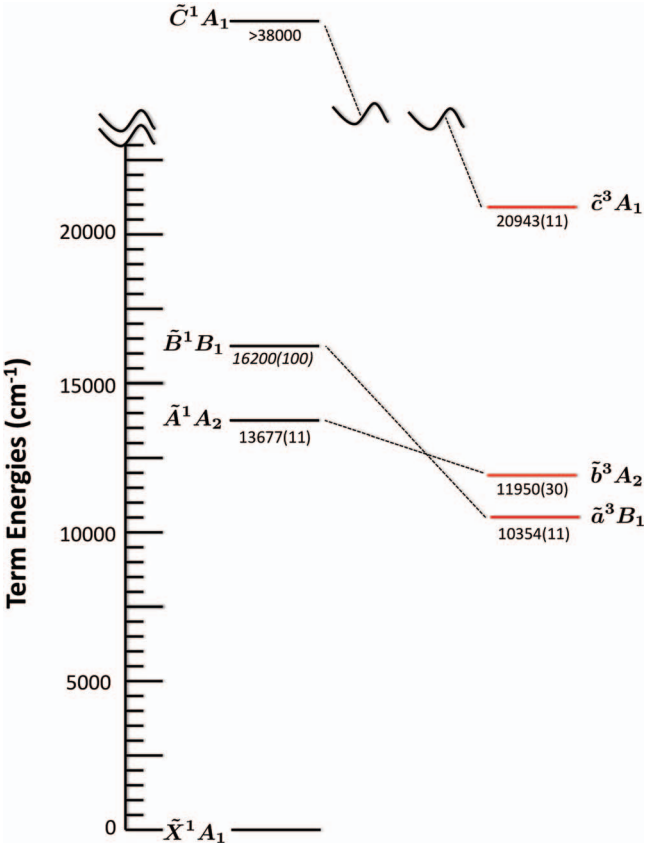

FIG. 3. Energy level diagram for the electronic states of propadienylidene. All energies are based on those determined in this research, except for that of the $\tilde{C}^1A_1$ state, which is taken from Refs. 18 and 72. The (italicized) energy for the $\tilde{B}^1B_1$ state is estimated by adjusting the measured position of its ν_2 level by the vibrational frequency, as estimated from the calculations. Note the marked difference in singlet–triplet splittings of the excited states, which are represented by the dotted lines. The ground state is obtained by removal of the $2b_1$ electron from the anion (see Fig. 2); excited A_2, B_1, and A_1 states are obtained by removal of the $2b_2$, $7a_1$, and $1b_1$ electrons, respectively.

spectrum near 28 000 cm^{-1}, but again the vibrational progressions associated with these transitions are hard to tease out of the spectra for reasons of both signal strength and the inherent difficulties associated with vibronic coupling. A very weak feature just below 33 000 cm^{-1} is assigned to a vibronic band associated with the $\tilde{B}^1B_1$ state (2_0^1), which corresponds to the strongest feature in the corresponding region of the optical spectrum; the $\tilde{B}^1B_1$ origin is problematic even in definition and its position is not established here. Above 35 000 cm^{-1}, the $\tilde{c}^3A_1$ state appears, which—unlike the states of A_2 and B_1 symmetry—is not strongly coupled to a nearby electronic state. Its vibrational progression is again apparent; and the representations of the molecular orbitals in Fig. 2 suggest that this state will have longer CC bonds than in the anion and that the dominant progression will be associated with q_4. The remaining state that corresponds to photodetachment from these frontier orbitals is the $\tilde{C}^1A_1$ state, which is known from optical spectroscopy to be located roughly 15 000 cm^{-1} above the upper limit of the range of energies studied here and shown in Fig. 1.[9,17,18,72]

A final word here concerns the splittings of the two vibronically coupled pairs of states: $\tilde{A}^1A_2$ and $\tilde{B}^1B_1$ as well as $\tilde{a}^3B_1$ and $\tilde{b}^3A_2$ (see Fig. 3). The present and previous results leave no doubt that the B_1 state is the lower triplet and the higher singlet, which shows that—despite the similarities in electronic structure—the singlet–triplet splitting is markedly larger for the B_1 pair of states than for the A_2 states. This can be rationalized as follows: in the A_2 states the two unpaired electrons are associated with π orbitals that have nodes perpendicular to, and in, the molecular plane, while in the B_1 states, the two orbitals are the perpendicular π orbital and a rather diffuse orbital loosely associated with the lone-pair on the outer carbon (C_3). The electrons therefore avoid one another somewhat better in the A_2 states, and the singlet–triplet splitting is correspondingly smaller for this reason. The excited A_1 states, $\tilde{c}^3A_1$ and $\tilde{C}^1A_1$, where the singlet–triplet splitting is very large, suffer from having the two unpaired orbitals in π orbitals with the same general orientation in the molecular frame.

We now proceed to discuss the NIPES, VMI, and SEVI spectra in greater detail.

B. The $\tilde{X}^1A_1$ electronic state

The $\tilde{X}^1A_1$ range of the photodetachment spectrum was recorded long ago by Robinson *et al.*[26] as well as by Oakes and Ellison.[25] In the course of the present research, this region of the spectrum has been rerecorded in the NIPES laboratory, and has also been measured with higher resolution using the SEVI method. While a detailed assignment of the spectrum has not previously been given, such an undertaking is largely straightforward. The current experimental spectra are shown in Figs. 4 and 5, along with the stick spectrum from the model Hamiltonian (which, for this state, is equivalent to an anharmonic Franck-Condon calculation). The origin found by SEVI is at eBE = 14 483 ± 8 cm^{-1} (1.7957 ± 0.0010 eV), which agrees with the previously reported EAs of 1.794 ± 0.008 eV by Robinson *et al.* and 1.794 ± 0.025 eV from Ref. 25 and gives a quite precise EA for propadienylidene. We now turn to the observed vibrational structure.

The small peak 412 ± 11 cm^{-1} above the $\tilde{X}^1A_1$ origin is readily assigned to the $2\nu_6$ level. The position is entirely consistent with the CCSD(T)/ANO1 calculated harmonic frequency for this mode, and there are no other plausible candi-

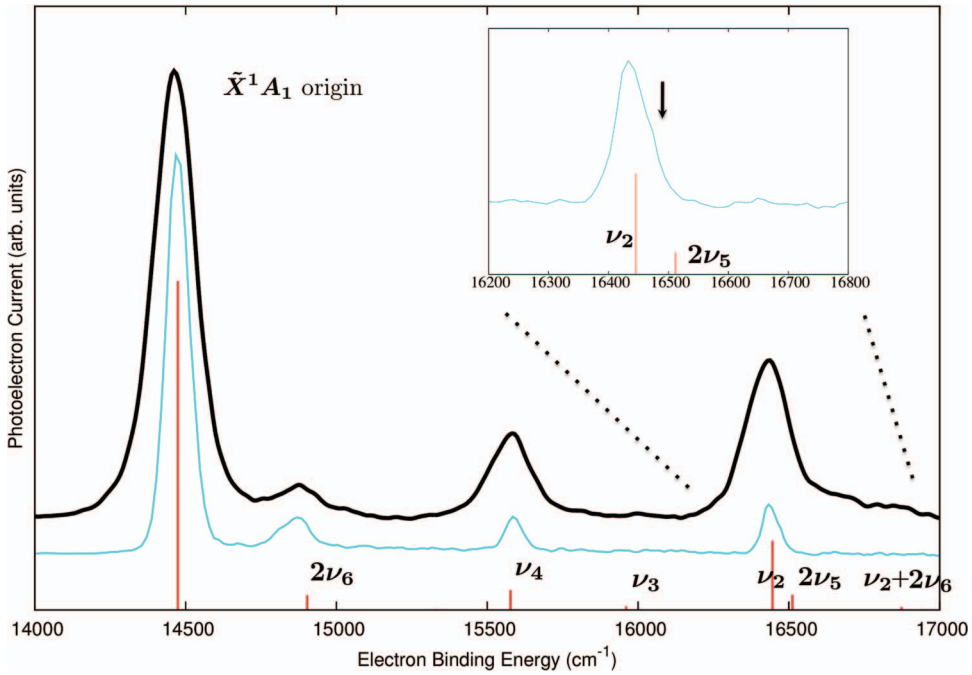

FIG. 4. Photoelectron spectra of H_2CCC^- from eBE = 14 000 to 17 000 cm^{-1}. The upper black trace is the 364-nm NIPES spectrum; the lower cyan trace is the SEVI data, obtained with a photon energy of 17 790 cm^{-1}. The red sticks along the baseline are from a Franck-Condon simulation, based on the corresponding diagonal block of the effective Hamiltonian used here. The eigenvalues of the model Hamiltonian have been shifted so that the origin feature coincides with that seen experimentally.

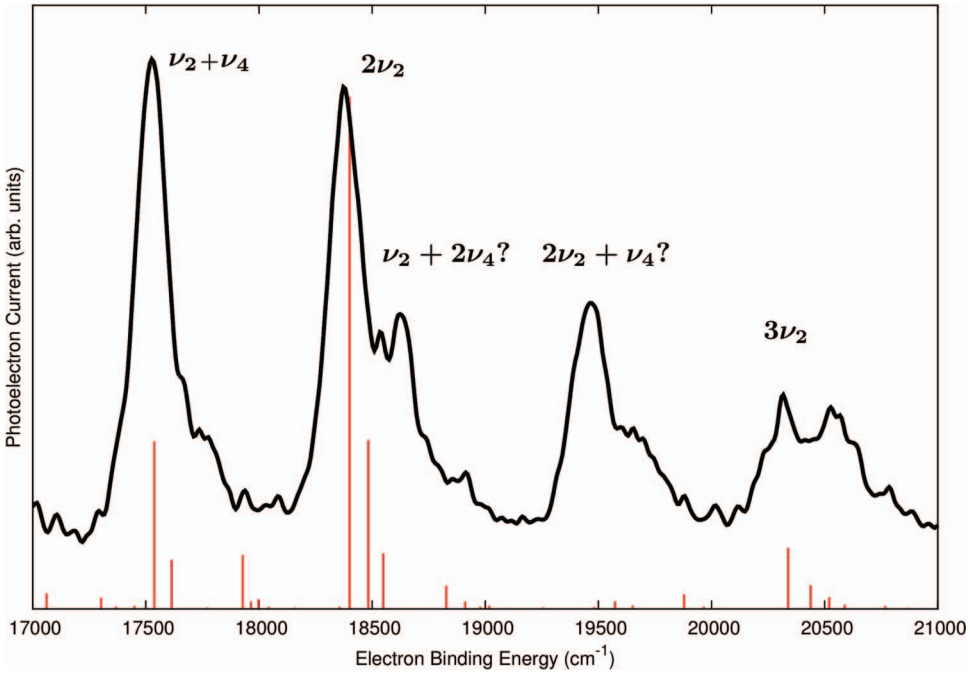

FIG. 5. Photoelectron spectra of H_2CCC^- from eBE = 17 000 to 21 000 cm^{-1}. The upper black trace is the 364-nm NIPES spectrum, and the red sticks from the Franck-Condon calculation are shown. The shift of the model Hamiltonian eigenvalues is as described in Fig. 4. The large number of prominent states in the stick spectrum are various combinations of the Franck-Condon active ν_2, ν_3, and ν_4 modes, together with even quantum levels involving ν_5 and ν_6.

dates for the carrier of this spectral feature. Moving to higher energies, the peaks seen at +1111 ± 11 and +1956 ± 11 cm^{-1} are clearly the ν_4 and ν_2 fundamentals, respectively.[73] The position of ν_2 is in excellent agreement with the strong infrared absorption seen at 1952 cm^{-1} in frozen argon and previously assigned to ν_2.[9–11] We are unaware of any previous assignments for the ν_4 mode (or, for that matter, any gas-phase vibrational assignments for H_2CCC), but are confident in our conclusion that $\nu_4 = 1111 \pm 11$ cm^{-1}. The assignments above are supported by the Franck-Condon simulation (see Fig. 4) and the CCSD(T) anharmonic frequencies (see Table V), but could easily have been made without either of them. The remainder of the spectrum could scarcely be properly interpreted without the simulations, however, as will become evident.

The ν_2 peak in the NIPES spectrum is accompanied by a tail towards the higher eBE side (see Fig. 4 as well as the corresponding region in Fig. 1), implying manifestation of another vibronic level in this energy region. Indeed, the spectral simulation predicts a small contribution from the $2\nu_5$ level at a slightly higher eBE than that for the ν_2 fundamental level. The ν_5 mode has b_1 symmetry and represents the out-of-plane wagging motion of the methylene group. The *ab initio* harmonic vibrational analysis yields quite different frequencies for this mode between the anion and $\tilde{X}^1A_1$ H_2CCC (see Table IV), which accounts for the significant Franck-Condon activity for the two-quantum level. The limited resolution of the NIPES measurements prevents accurate determination of the $2\nu_5$ level energy, but the simulated spectrum is consistent with the NIPES spectrum.[74]

Due to its higher resolution, the ν_2 peak in the SEVI spectrum has a much narrower line width than that in the NIPES spectrum. A close inspection, however, reveals that the higher eBE side of the SEVI peak slopes slightly more gradually than the lower eBE side, with a small shoulder in the middle (see inset in Fig. 4). This observation appears to be in accordance with that made in the NIPES measurements and further corroborates the presence of the $2\nu_5$ peak. The level energy is determined to be +1990 ± 50 cm^{-1} from these measurements; it is in excellent agreement with the CCSD(T)/ANO1 calculations (VPT2, see Table V).

Looking at Fig. 5, things are relatively clear up to about 4500 cm^{-1} above the $\tilde{X}^1A_1$ origin. A peak around eBE = 17 560 cm^{-1} is rather easily attributed to the combination of the Franck-Condon active modes ν_2 and ν_4 ($\nu_2 + \nu_4$ = 3077 ± 80 cm^{-1}), while that near 18 400 cm^{-1} (+3940 ± 100 cm^{-1}) is the $2\nu_2$ level. Interestingly, the Franck-Condon simulation contains no obvious level to associate with the band seen around eBE = 19 500 cm^{-1}, which is 5020 ± 80 cm^{-1} above the origin. The only vibrational level given by the VPT2 calculation that is both within the neighborhood

TABLE V. Assigned vibrational levels in the ground $\tilde{X}^1A_1$ electronic state of propadienylidene. All energies are in units of cm^{-1}.

Level	VPT2 estimate	Peak center
ν_2	1953	1956 ± 11
ν_4	1105	1111 ± 11
$2\nu_6$	443	412 ± 11
$2\nu_5$	2000	1990 ± 50
$\nu_2 + \nu_4$	3040	3077 ± 80
$2\nu_2$	3887	3940 ± 100
$\nu_2 + 2\nu_4$	4122	4180 ± 80
$2\nu_2 + \nu_4$	4955	5020 ± 80
$3\nu_2$	5800	5900 ± 150

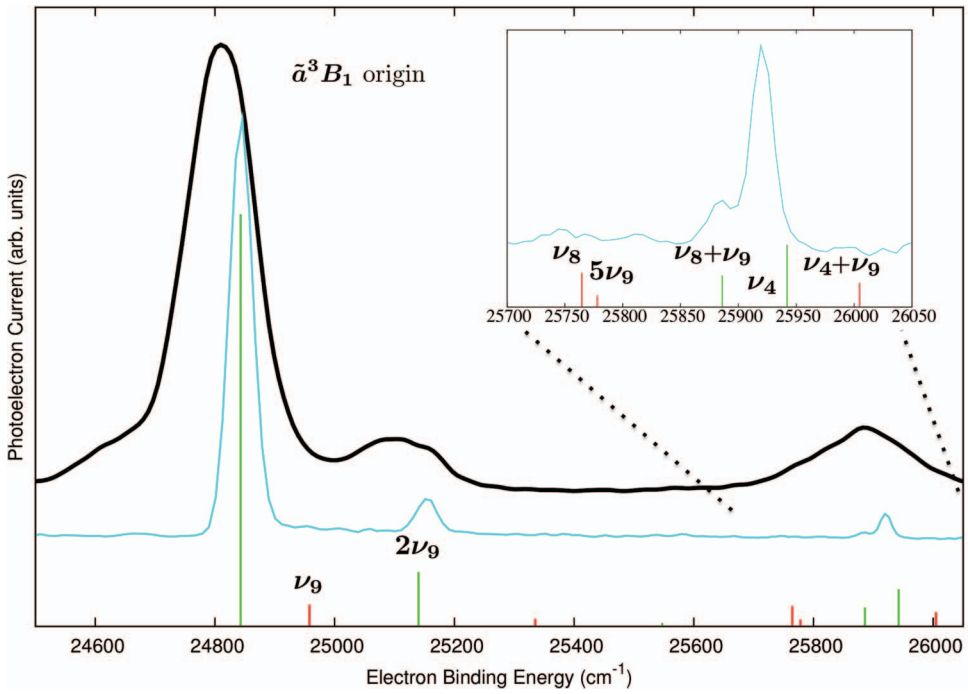

FIG. 6. Photoelectron spectra of H_2CCC^- from eBE = 24 500 to 26 050 cm^{-1}. The upper black trace is the NIPES spectrum; the lower cyan trace is the SEVI spectrum, obtained with a photon energy of 26 450 cm^{-1}. Green and red sticks shown along the baseline are vibronic levels with b_1 and a_2 vibronic symmetries, respectively, as obtained from the model Hamiltonian assuming equal photodetachment cross sections for the $\tilde{a}^3B_1$ and $\tilde{b}^3A_2$ electronic states. Nominal vibrational quantum numbers are also given, and all states in this range can be assigned as vibrational levels of the $\tilde{a}^3B_1$ state. The simulation has been shifted so that the $\tilde{a}^3B_1$ origin feature coincides with that seen in the SEVI experiment.

energetically *and* a plausible candidate for Franck-Condon activity is $2\nu_2 + \nu_4$, and we tentatively make this assignment. Going yet further in the singlet spectrum, one can only say that $3\nu_2$ is associated with one of the features near eBE = 20 500 cm^{-1}; a remaining peak (not shown in Fig. 5) between eBE = 21 000 and 22 000 cm^{-1} is too broad to yield to meaningful analysis. The assignments involving the $\tilde{X}^1A_1$ state are summarized in Table V, along with the corresponding level positions obtained in the VPT2 calculation.

C. Triplet states

1. $\tilde{a}^3B_1$ and $\tilde{b}^3A_2$ states

The earlier photoelectron spectrum[26] of the $\tilde{X}^2B_1$ state of the propadienylidene anion revealed peaks at low eKE that have been attributed to the lowest triplet state. This lowest triplet predicted by *ab initio* calculations is the $\tilde{a}^3B_1$ state. The term energy ($T_0 = 1.288 \pm 0.009$ eV; 10 390 ± 70 cm^{-1}) inferred from the earlier measurement is in agreement with the present higher-resolution SEVI data (see Fig. 6), which give T_0 = 1.2837 ± 0.0014 eV (10354 ± 11 cm^{-1}). Beyond the term energy, however, no spectroscopic constants were determined in the work of Robinson *et al.*,[26] although two weak features were observed and documented ∼300 and 1050 cm^{-1} above the $\tilde{a}^3B_1$ origin. Both of these features are clearly seen in the SEVI experiment. The lower energy peak is found at +313 ± 11 cm^{-1} (relative to the $\tilde{a}^3B_1$ origin), while that at the higher energy appears to be a doublet, with two components at approximately +1050 and +1085 cm^{-1}. At yet higher energies in this region, no unambiguous levels are seen in the SEVI spectrum until a fairly prominent peak at eBE = 28160 ± 8 cm^{-1}, which is some 3300 cm^{-1} above the $\tilde{a}^3B_1$ origin and is assigned to a higher-lying singlet state (see Sec. IV D).

Turning now to the calculations performed at the CCSD(T)/ANO1 level, one finds support for assignment of the strong peak to the origin of the $\tilde{a}^3B_1$ state; the calculations predict a term energy within 0.05 eV of the observed origin position (see Table IV). Inspection of the harmonic frequencies predicted by theory reveals only two plausible candidates for the peak seen at +313 ± 11 cm^{-1}, specifically $2\nu_9$ or the ν_6 fundamental. The latter seems unlikely because this mode has b_1 symmetry and its presence in the spectrum would require coupling of the $\tilde{a}^3B_1$ state with a higher state of $^3A_1$ electronic symmetry,[75] thus the $2\nu_9$ level is assigned[76] to the feature at +313 cm^{-1}.

The feature(s) just below eBE = 26 000 cm^{-1} do not represent any real challenge to assignment (see Table VI). The fact that the equilibrium geometry predicted for the $\tilde{a}^3B_1$ state is displaced from the anion principally along coordinate q_4 (see Table IV) suggests that Franck-Condon activity in ν_4 will be observed. And indeed, the harmonic frequency calculated for this mode (1096 cm^{-1}) is consistent with the observed stronger feature at approximately +1080 cm^{-1}. The origin of the doubling of this feature is less obvious, but can ultimately be attributed to a Fermi resonance with $\nu_8 + \nu_9$.[77]

Above 26 000 cm^{-1}, things are significantly more complicated. Figure 7 shows two SEVI and one VMI spectra, obtained with photon energies of 27 550, 31 740, and

TABLE VI. Observed features and assignments for the ground vibronic state and selected excited state levels of H_2CCC in the photoelectron spectrum of H_2CCC^-. All energies in cm^{-1}, with reported uncertainties of $\sim 1\sigma$. While the various experimental results are consistent within the indicated uncertainty, the recommended values are shown in boldface. Energies in the upper row are the electron binding energies (relative to the ground state of the anion); italicized values in the row below are relative to the ground vibronic level of the neutral.

NIPES and VMI data		SEVI data		
Position	Uncertainty	Position	Uncertainty	Assignment
14 470	30	**14 483**	**8**	$\tilde{X}^1A_1$ origin
24 809	50	**24 837**	**8**	$\tilde{a}^3B_1$ origin
10 339	*60*	***10 354***	***11***	
25 100	50	**25 150**	**8**	$2\nu_9(\tilde{a}^3B_1)$
10 630	*60*	***10 677***	***11***	
		25 885	**8**	$\nu_8 + \nu_9(\tilde{a}^3B_1)$
		11 402	***11***	
25 882	50	**25921**	**8**	$\nu_4(\tilde{a}^3B_1)$
11 412	*60*	***11 438***	***11***	
26 366	60	**26 433**	**20**	$\tilde{b}^3A_2$ origin
11 896	*70*	***11 950***	***22***	
26 672	**60**			$2\nu_9(\tilde{b}^3A_2)$
12 202	***70***			
27 000	**60**			see text
12 530	***70***			
28 164	50	**28 160**	**8**	$\tilde{A}^1A_2$ origin
13 694	*60*	***13 677***	***11***	
29 721	**80**			ν_2 $(\tilde{A}^1A_2)$
15 151	***90***			
32 786	**50**			ν_2 $(\tilde{B}^1B_1)$
18 316	***60***			
35 416	40	**35 426**	**8**	$\tilde{c}^3A_1$ origin
20 946	*50*	***20 943***	***11***	
36 375	**40**			ν_4 $(\tilde{c}^3A_1)$
21 905	***50***			

32 260 cm^{-1}, respectively. Probably due to the fact that the VMI spectrum is farther from threshold than the lower-energy SEVI spectrum, three features beyond the peak that corresponds to ν_4 in the $\tilde{a}^3B_1$ state are much more easily seen in the VMI spectrum.[78] Given that the $\tilde{b}^3A_2$ state is calculated to be about 2000 cm^{-1} above the $\tilde{a}^3B_1$ state, this is precisely the region where the origin of the former should be found. The simulated spectrum from the model Hamiltonian, which is shown in red, provides the best way to interpret this region.[79] There is a great deal of congestion (see the stick spectrum) that results from the strong vibronic coupling between the two low-lying triplet states. The first feature with a_2 vibronic symmetry and appreciable intensity would appear to correspond to the first of the three weak maxima beyond the ν_4 peak of the $\tilde{a}^3B_1$ state near 26 400 cm^{-1}, and this is accordingly assigned to the origin of the $\tilde{b}^3A_2$ state. While barely perceptible from the noise in the 28 000 cm^{-1} SEVI spectrum, there is a reproducible albeit quite weak feature seen at 26 433 cm^{-1}, from which the term energy of the $\tilde{b}^3A_2$ state can be estimated as 11 950 $\pm$ 30 cm^{-1}. From the simulation, the weak feature some 300 cm^{-1} above the $\tilde{b}^3A_2$ origin (eBE $\sim$ 26 750 cm^{-1}) appears to be dominated by a vibronic level also having a_2 symmetry; analysis of the nodal properties of the vibronic wavefunction associated with this state reveals it to be best described as the $2\nu_9$ level within the $\tilde{b}^3A_2$ state. The fourth, and weakest, peak shown in Fig. 7 at an eBE near 27 000 cm^{-1}, while plausibly reproduced by the simulation, clearly cannot be associated with any particular level(s). Several vibronic states contribute to the simulated spectrum in this area, and a similarly complex mixing of states is likely responsible for the experimental peak.[80]

In contrast to the weak signals in the region of the $\tilde{b}^3A_2$ origin, a more prominent peak—and one clearly seen in the SEVI spectrum—is found about 1700 cm^{-1} above that which has been assigned to the $\tilde{b}^3A_2$ origin. The separation, as deduced from the two SEVI traces is 1727 $\pm$ 11 cm^{-1}, and it might be tempting to assign this as "ν_2" of the $\tilde{b}^3A_2$ state (see Ref. 80). However, things are not so straightforward. First of all, the simulation indicates a pronounced splitting of ν_2 into several different vibronic components, with none of these clearly identifiable as a well-defined and unique ν_2 state. This feature of the spectrum is qualitatively similar to what is seen in the $\tilde{B}^1B_1 \leftarrow \tilde{X}^1A_1$ absorption spectrum, again due to strong vibronic coupling between $\tilde{A}^1A_2$ and $\tilde{B}^1B_1$ states. Also, it is interesting to note that the short (outer) C–C bond length in the $\tilde{b}^3A_2$ state is the longest of the six electronic states under study and correspondingly has the smallest ν_2 frequency of all electronic states studied here. The harmonic level is calculated to be at 1637 cm^{-1}, which is roughly 100 cm^{-1} below the rather sharp maximum seen in the SEVI spectrum at an eBE of 28 160 cm^{-1}. It is more likely that this rather strong feature has contributions from *both* "ν_2" in the $\tilde{b}^3A_2$ state and the first excited singlet state (see Sec. IV D), with the latter contribution dominating.

2. The $\tilde{c}^3A_1$ state

Unlike the strongly coupled $\tilde{a}^3B_1$ and $\tilde{b}^3A_2$ states, which leave a rather complex spectral signature, the higher-lying $\tilde{c}^3A_1$ state appears to display quite straightforward Franck-Condon activity only. The origin of this state is found by SEVI at 35 426 $\pm$ 8 cm^{-1} corresponding to a term energy of 20 943 $\pm$ 11 cm^{-1}, which is in good agreement with the (harmonic) zero-point corrected calculated value of 20 863 cm^{-1}. A pronounced vibrational progression is seen (Fig. 8) in the ν_4 mode, as is expected from the large geometry difference in this mode (see Table IV). The spacing is roughly 950 cm^{-1}, this being consistent with the calculated harmonic frequency of 938 cm^{-1}. Beyond assigning the fundamental of ν_4 to the first maximum with appreciable intensity at 960 $\pm$ 50 cm^{-1} above the origin, things are complicated by mode-mode coupling. There is a Fermi resonance between $2\nu_4$ and ν_2 (see both the harmonic frequencies in Table IV and the simulated stick spectrum in Fig. 8), so that both of these levels—which are also associated with non-negligible Franck-Condon activity—likely contribute to the next member of the progression.

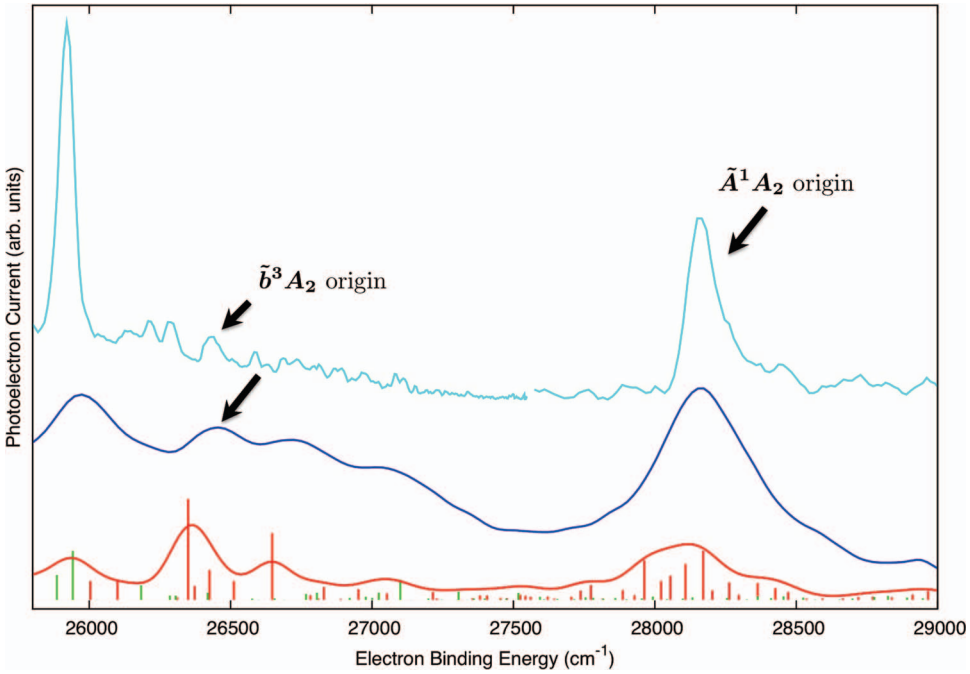

FIG. 7. Photoelectron spectra of H_2CCC^- from eBE = 25 800 to 29 000 cm^{-1}. The cyan trace is the SEVI data obtained at photon energies of 27 550 cm^{-1} and 31 740 cm^{-1}, with the boundary between the two clearly demarcated. The lower blue trace is the VMI spectrum obtained with a photon energy of 32 260 cm^{-1} (4.0 eV). The stick spectrum, obtained from the model Hamiltonian, is shown along the baseline, with red sticks indicating levels with a_2 vibronic symmetry and green indicating b_1 vibronic symmetry. The dominant lower energy peak in the spectrum is the ν_4 band of the $\tilde{a}^3B_1$ state which is also seen in the preceding figure; the position of the apparent $\tilde{b}^3A_2$ origin is indicated with an arrow. The shift applied to the calculated spectrum is the same as that used in Figure 4. The red trace is obtained from the model Hamiltonian spectrum, with each peak in the stick spectrum convoluted with a Gaussian with FWHM 40 cm^{-1}.

D. The $\tilde{A}^1A_2$ and $\tilde{B}^1B_1$ singlet states

The peak mentioned towards the end of Sec. IV C 1—seen at an eBE of 28 160 ± 8 cm^{-1} in the SEVI spectrum—is assigned to the origin of the $\tilde{A}^1A_2$ state.[81] From this peak position, one can extract a term energy of T_0= 13 677 ± 11 cm^{-1} for the $\tilde{A}^1A_2$ state. As manifest in the simulated spectrum (see Figs. 9 and 10), the vibronic interaction tends to "spread out" the $\tilde{B}^1B_1$ origin. What one might expect to see

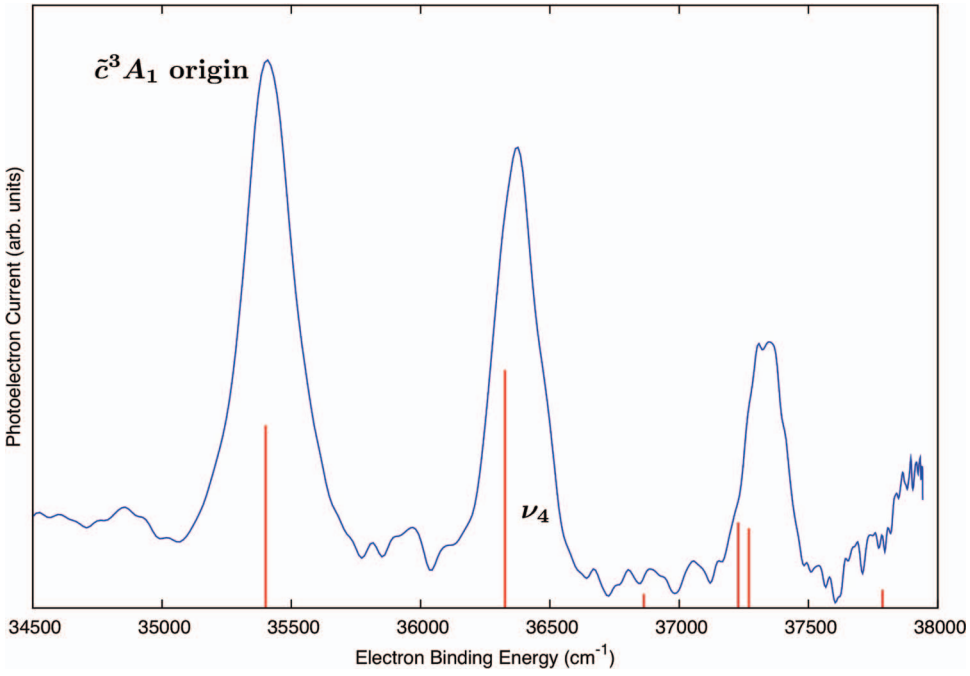

FIG. 8. Photoelectron VMI spectrum of H_2CCC^- from eBE =34 500 to 38 000 cm^{-1} obtained with a photon energy of 37 940 cm^{-1}. Along the baseline is a stick spectrum obtained from the model Hamiltonian in the Franck-Condon approximation. Note the resonance between ν_2 and $2\nu_4$ that results in the polyad structure of the spectrum.

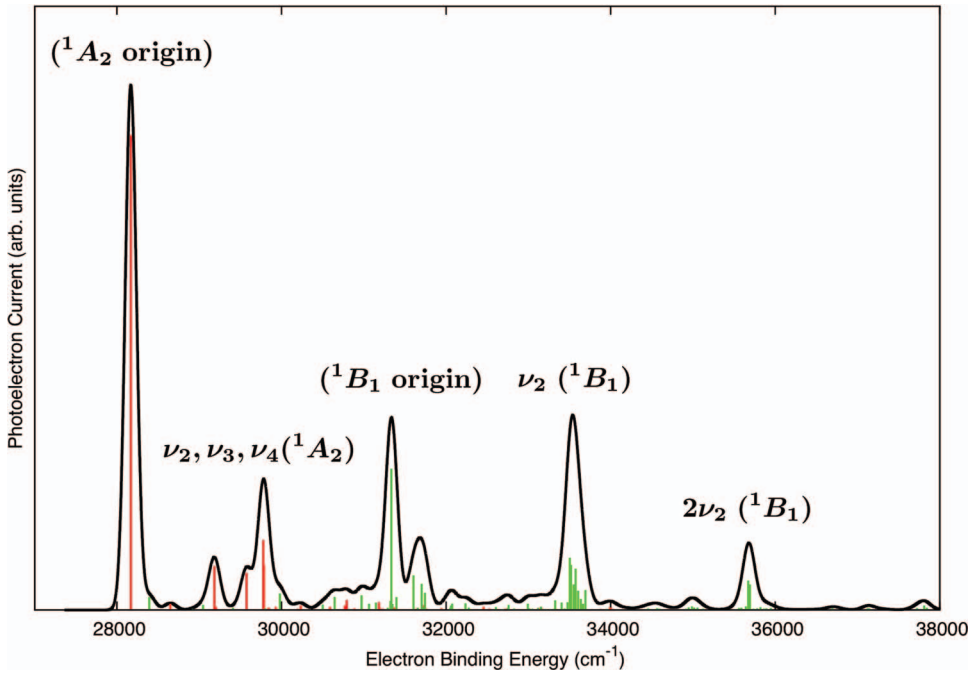

FIG. 9. Simulated photoelectron spectrum of H_2CCC^- to the $\tilde{A}^1A_2$ and $\tilde{B}^1B_1$ states of H_2CCC, as calculated from the purely *ab initio* Hamiltonian (the relative energies of the two neutral states are unadjusted). Red sticks correspond to vibronic levels of a_2 symmetry, while the green sticks indicate b_1 vibronic levels. Due to the strong vibronic coupling that mixes these two states, only the $\tilde{A}^1A_2$ origin has a "clean" assignment; general assignments of the various features are given in the figure. The energy range shown extends just beyond what roughly corresponds to the $3\nu_2$ vibrational level in the $\tilde{B}^1B_1$ state, which exhibits very little activity. At higher energies, no significant features are present. The simulated spectrum has been shifted so that the $\tilde{A}^1A_2$ origin is coincident with the T_0 feature measured by SEVI.

are perhaps four additional spectroscopic features: one that can be loosely associated with vibrational levels in the $\tilde{A}^1A_2$ state some 1500 cm^{-1} above the strong origin band, another in the vicinity of the $\tilde{B}^1B_1$ "origin" (and similar in general appearance to that seen in the absorption spectrum[18,19,24]) and then two more: a moderately stronger peak that would be associated with ν_2 in the $\tilde{B}^1B_1$ state and the associated $2\nu_2$ level (see Fig. 9, noting that this figure shows *only* the simulated spectrum and no experimental data). The ν_2 band corresponds to the strongest peak in the electronic absorption spectrum, that which has been postulated to be responsible for the DIB at 5450 Å. Beyond those mentioned above, the simulation suggests that there will be only weak features; the level of activity in the ν_2 mode is less than that in absorption.[82] Also, ν_4, which is somewhat Franck-Condon active in the absorption spectrum, is similarly inconspicuous in the simulation. Both of these qualitative factors are expected, given the normal coordinate displacements that are documented for the relevant states in Table IV.

The VMI spectrum, taken at a photon energy of 33 590 cm^{-1}, is shown together with the simulated spectrum in Fig. 10. In this figure, the simulated spectrum is calculated from the model Hamiltonian but with the vertical gap between the $\tilde{A}^1A_2$ and $\tilde{B}^1B_1$ states reduced by 800 cm^{-1}. Apart from the $\tilde{A}^1A_2$ origin, the experimental signal is not really sufficient to reveal many of the features predicted in the simulation. There is, indeed, a reproducible maximum 1557 ± 90 cm^{-1} (eBE = 29 717 ± 90 cm^{-1}) above the $\tilde{A}^1A_2$ origin feature, which can be loosely associated with the ν_2 level in the $\tilde{A}^1A_2$ state. Above this, another feature is seen around +2500 cm^{-1} relative to the $\tilde{A}^1A_2$ origin, which—again loosely—comprises the elusive (even in definition of Ref. 19) $\tilde{B}^1B_1$ origin level. There is, however, a fairly well-resolved and conspicuous band at +4621 ± 50 cm^{-1} (clearly seen in the overview spectrum, Fig. 1) that we assign to the cluster of vibronic levels near ν_2 of the $\tilde{B}^1B_1$ state[83] (see simulation as well as Ref. 19). While there is another predicted band with appreciable intensity (that associated with the $2\nu_2$ level in the $\tilde{B}^1B_1$ state and potentially with the 4881 Å feature seen by CRDS), it would fall between the ranges pictured in Figs. 8 and 10, but is not resolvable in the current data.

V. ASTROPHYSICAL RELEVANCE OF EXCITED SINGLET STATES

That the $\tilde{A}^1A_2$ and $\tilde{B}^1B_1$ electronic states of propadienylidene are strongly mixed by the vibronic interaction and that the spectroscopic signature of this phenomenon can be seen at wavelengths between 400 and 650 nm has been appreciated for quite some time.[17–19,22–24] In addition to the fundamental chemical physics appeal, this particular band system has also been the source of a great deal of interest in the astrophysical community. As H_2CCC is the simplest stable[84] cumulene carbene, a class of molecules that were postulated long ago[85] as potential carriers of DIBs,[86] it has attracted wide interest since its discovery in the diffuse interstellar medium.[13] The fact that the visible absorption ultimately traced to the $\tilde{A}^1A_2$ and $\tilde{B}^1B_1$ states might be relevant for the DIBs was first pointed out in Ref. 18, but this idea has only been taken seriously in recent years. In a CRDS study,

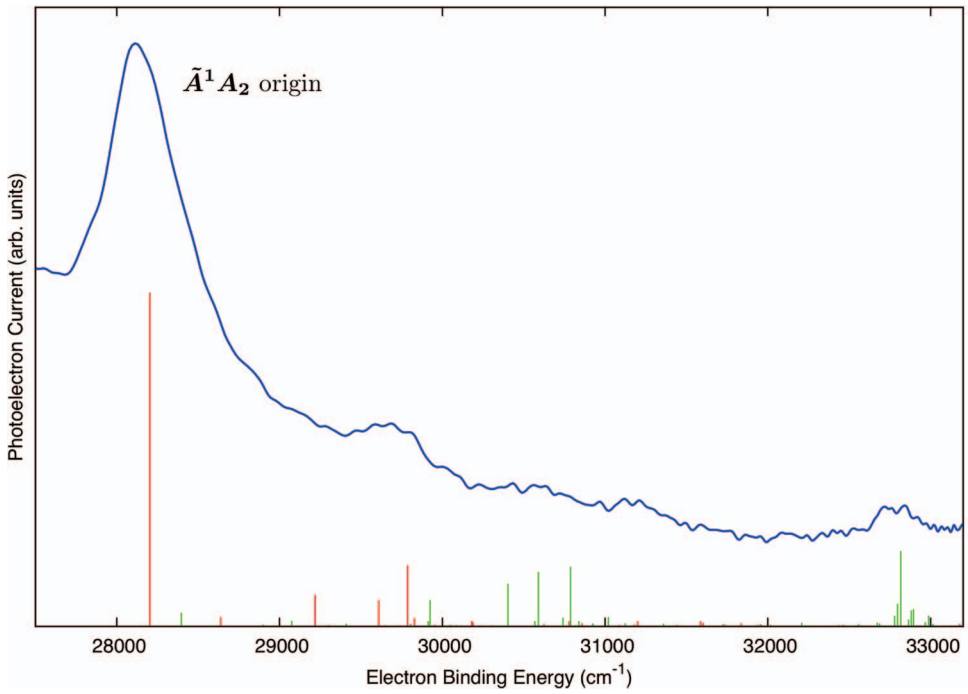

FIG. 10. Experimental VMI photoelectron spectrum of H_2CCC^- in the region of eBE = 27 500 to 33 200 cm^{-1}, obtained at a photon energy of 33 590 cm^{-1}. The stick spectrum (same color scheme as in Fig. 6) from the simulation is also shown, where the vertical gap between the $\tilde{A}^1A_2$ and $\tilde{B}^1B_1$ states has been shifted by −800 cm^{-1} (0.1 eV) due to the higher-order correlation effects that principally affect the $\tilde{B}^1B_1$ state (see text). Apart from moving the vibronic features associated with the $\tilde{B}^1B_1$ state to lower energy, note that shifting the gap has a profound effect on the intensity profile (see Fig. 9 for the unadjusted spectrum) in the vicinity of $\tilde{B}^1B_1$ origin.

Linnartz *et al.*[87] found a broad absorption feature centered near 5450 Å in an acetylene discharge, and noted a coincidence with a DIB. Although an effort to identify the molecular carrier was unsuccessful, they were able to show that it contained only carbon and hydrogen by varying the discharge conditions. This position is close to the strongest vibronic band observed in the propadienylidene $\tilde{A}^1A_2$ /$\tilde{B}^1B_1$ ←$\tilde{X}^1A_1$ band system in rare-gas matrices,[18,24] and it is well-established that H_2CCC is abundantly produced under these experimental conditions. Another gas-phase investigation including isotopic substitution of the electronic spectrum was undertaken with CRDS.[24] The feature at 5450 Å was again observed in this CRDS study, along with an additional absorption at 4881 Å which is also consistent, in terms of both position and profile, with another DIB.

Using results from this work, one can take the SEVI value for the EA (14 483 ± 8 cm^{-1}), and the position of the ν_2 band associated with the $\tilde{B}^1B_1$ state mentioned above (eBE = 32 786 ± 50 cm^{-1}) to determine that this level lies 18 303 ± 50 cm^{-1} above the ground $\tilde{X}^1A_1$ state, which is a range of energy that corresponds to photon wavelengths between 5448 and 5478 Å. Thus, the results are consistent with the contention that the persistent absorption centered at 5450 Å in acetylene discharges—and coincident in position and profile with a DIB—is due to propadienylidene.

VI. SUMMARY

In this study, a concerted experimental effort has been focused on locating the excited states of H_2CCC using negative ion photoelectron spectroscopy. The origin transitions for the $\tilde{X}^1A_1$ and $\tilde{a}^3B_1$ states have been observed with better resolution, and those for the $\tilde{b}^3A_2$, $\tilde{c}^3A_1$, and $\tilde{A}^1A_2$ states have been measured for the first time. Strong vibronic coupling exists between the electronic states of A_2 and B_1 spatial symmetries for both singlet and triplet spin configurations. The coupling between the singlet states has been known from the visible absorption spectrum of H_2CCC for quite some time (and is largely responsible for the fact that the $\tilde{B}^1B_1$ origin is not clearly observed here); the analogous coupling between the triplet states has been first observed here. All in all, six of the lowest seven electronic states of propadienylidene have been studied; the next excited electronic level is the $\tilde{C}^1A_1$ state, which lies well outside the energy range of experiments due to an extremely large singlet–triplet splitting of >2 eV for the A_1 symmetry states.

Finally, this work shows the power of combining different laboratory techniques to obtain a fairly high-resolution photoelectron spectrum over a wide range of energies. Further, this paper illustrates how theory can be combined with experiment to gain understanding into the assignments and qualitative observations, such as the large variation of singlet–triplet splittings found for the excited states of A_1, B_1, and A_2 electronic symmetries.

ACKNOWLEDGEMENTS

This work was supported by the U.S. National Science Foundation (NSF) (Grant Nos. PHY1125844 and CHE0809391 to W.C.L.; CHE1012743 to J.F.S.;

CHE1011959 to R.J.M.); the U.S. Air Force Office of Scientific Research (Grant No. F49620-03-1-0085 to D.M.N. and Grant No. FA9550-09-1-0046 to W.C.L.); the U.S. Department of Energy Basic Energy Sciences Division (Grant No. DE-FG02-07ER15884 to J.F.S.) and the Robert A. Welch Foundation (Grant No. F-1283 to J.F.S.). J.P.M. and D.L.O. are grateful for JILA Fellowships during 2011. D.L.O. is supported by the Division of Chemical Sciences, Geosciences, and Biosciences, the Office of Basic Energy Sciences, the U.S. Department of Energy. Sandia is a multi-program laboratory operated by Sandia Corporation, a Lockheed Martin Company, for the National Nuclear Security Administration. We would also like to thank M. C. McCarthy (Harvard) and Tim Schmidt (Sydney) for discussions and their interest in this work.

[1] C. A. Taatjes, S. J. Klippenstein, N. Hansen, J. A. Miller, T. A. Cool, J. Wang, M. E. Law, and P. R. Westmoreland, Phys. Chem. Chem. Phys. **7**, 806 (2005).
[2] P. Maksyutenko, F. Zhang, X. Gu, and R. I. Kaiser, Phys. Chem. Chem. Phys. **13**, 240 (2011).
[3] "Special Issue: Titan Atmosphere" J. Phys. Chem. A **113**, 11097 (2009).
[4] "Special Issue: Progress in Understanding Titan's Atmosphere and Space Environment" Philos. Trans. R. Soc. London, Ser. A **367**, 603 (2009).
[5] R. Lorenz and J. Mitton, *Titan Unveiled: Saturn's Mysterious Moon Explored* (Princeton University Press, Princeton, 2008).
[6] P. Thaddeus and M. C. McCarthy, Spectrochim. Acta **57A**, 757 (2001).
[7] E. Herbst, Chem. Soc. Rev. **30**, 168 (2001).
[8] P. Ehrenfreund and S. B. Charnley, Annu. Rev. Astron. Astrophys. **38**, 427 (2000).
[9] R. A. Seburg, E. V. Patterson, J. F. Stanton, and R. J. McMahon, J. Am. Chem. Soc. **119**, 5847 (1997).
[10] G. Maier, H. P. Reisenauer, W. Schwab, P. Čársky, B. A. Hess, Jr., and L. J. Schaad, J. Am. Chem. Soc. **109**, 5183 (1987).
[11] G. Maier, H. P. Reisenauer, W. Schwab, P. Čársky, V. Špirko, B. A. Hess, Jr., and L. J. Schaad, J. Chem. Phys. **91**, 4763 (1989).
[12] J. M. Vrtilek, C. A. Gottlieb, E. W. Gottlieb, T. C. Killian, and P. Thaddeus, Astrophys. J. **364**, L53 (1990).
[13] J. Cernicharo, C. A. Gottlieb, M. Guélin, T. C. Killian, G. Paubert, P. Thaddeus, and J. M. Vrtilek, Astrophys. J. **368**, L39 (1991).
[14] C. A. Gottlieb, T. C. Killian, P. Thaddeus, P. Botschwina, J. Flügge, and M. Oswald, J. Chem. Phys. **98**, 4478 (1993).
[15] M. C. McCarthy and P. Thaddeus, J. Mol. Spectrosc. **211**, 235 (2002).
[16] J. Gauss and J. F. Stanton, J. Mol. Struct. **485**, 43 (1999).
[17] J. F. Stanton, J. T. DePinto, R. A. Seburg, J. A. Hodges, and R. J. McMahon, J. Am. Chem. Soc. **119**, 429 (1997).
[18] J. A. Hodges, R. J. McMahon, K. W. Sattelmeyer, and J. F. Stanton, Astrophys. J. **544**, 838 (2000).
[19] J. F. Stanton, Faraday Discuss. **150**, 331 (2011).
[20] R. A. Seburg and R. J. McMahon, Angew. Chem. Int. Ed. Engl. **34**, 2009 (1995).
[21] *The Diffuse Interstellar Bands*, edited by A. G. G. M. Tielens and T. P. Snow (Kluwer, Dordrecht, 1995).
[22] P. Birza, A. Chirokolava, M. Araki, P. Kolek, and J. P. Maier, J. Mol. Spectrosc. **229**, 276 (2005).
[23] E. Achkasova, M. Araki, A. Denisov, and J. P. Maier, J. Mol. Spectrosc. **237**, 70 (2006).
[24] J. P. Maier, G. A.H. Walker, D. A. Bohlender, F. J. Mazzotti, R. Raghunandan, J. Fulara, I. Garkusha, and A. Nagy, Astrophys. J. **726**, 41 (2011).
[25] J. M. Oakes and G. B. Ellison, Tetrahedron **42**, 6263 (1986).
[26] M. S. Robinson, M. L. Polak, V. M. Bierbaum, C. H. DePuy, and W. C. Lineberger, J. Am. Chem. Soc. **117**, 6766 (1995).
[27] K. M. Ervin and W. C. Lineberger, in *Advances in Gas Phase Ion Chemistry*, edited by N. G. Adams and L. M. Babcock (JAI, Greenwich, 1992), Vol. 1, pp. 121–166.
[28] L. Sheps, E. M. Miller, and W. C. Lineberger, J. Chem. Phys. **131**, 064304 (2009).
[29] D. M. Neumark, J. Phys. Chem. A **112**, 13287 (2008).
[30] E. P. Wigner, Phys. Rev. **73**, 1002 (1948).
[31] D. G. Leopold, K. K. Murray, A. E. Stevens Miller, and W. C. Lineberger, J. Chem. Phys. **83**, 4849 (1985).
[32] K. M. Ervin, J. Ho, and W. C. Lineberger, J. Chem. Phys. **91**, 5974 (1989).
[33] S. W. Wren, K. M. Vogelhuber, J. Garver, S. Kato, L. Sheps, V. M. Bierbaum, and W. C. Lineberger, "C–H bond strengths and acidities in aromatic systems: Effects of nitrogen incorporation in mono-, di-, and triazines," J. Am. Chem. Soc. (submitted).
[34] J. Cooper and R. N. Zare, J. Chem. Phys. **48**, 942 (1968).
[35] C. S. Feigerle, Ph.D. dissertation (University of Colorado, 1983).
[36] D. M. Neumark, K. R. Lykke, T. Anderson, and W. C. Lineberger, Phys. Rev. A **32**, 1890 (1985).
[37] T. Sanford, S.-Y. Han, M. A. Thompson, R. Parson, and W. C. Lineberger, J. Chem. Phys. **122**, 054307 (2005).
[38] M. A. Johnson and W. C. Lineberger, in *Techniques for the Study of Ion-Molecule Reactions*, edited by J. M. Farrar and W. H. Saunders, Jr. (Wiley, New York, 1988), pp. 591–635.
[39] W. C. Wiley and I. H. McLaren, Rev. Sci. Instrum. **26**, 1150 (1955).
[40] D. W. Chandler and P. L. Houston, J. Chem. Phys. **87**, 1445 (1987).
[41] A. T. J. B. Eppink and D. H. Parker, Rev. Sci. Instrum. **68**, 3477 (1997).
[42] K. Yokoyama, G. W. Leach, J. B. Kim, and W. C. Lineberger, J. Chem. Phys. **105**, 10696 (1996).
[43] D. L. Osborn, K. M. Vogelhuber, S. W. Wren, E. M. Miller, Y.-J. Lu, A. S. Case, R. J. McMahon, and W. C. Lineberger, "Electronic states of the quasi-linear molecule propargylene (HCCCH) from negative ion photoelectron spectroscopy" (unpublished).
[44] W. H. Robertson, J. A. Kelley, and M. A. Johnson, Rev. Sci. Instrum. **71**, 4431 (2000).
[45] D. Hanstorp and M. Gustafsson, J. Phys. B **25**, 1773 (1992).
[46] C. E. Moore, *Atomic Energy Levels* (National Bureau of Standards, Washington, D.C., 1949), Vol. I.
[47] C. E. Moore, *Atomic Energy Levels* (National Bureau of Standards, Washington, D.C., 1949), Vol. III.
[48] A. Osterwalder, M. J. Nee, J. Zhou, and D. M. Neumark, J. Chem. Phys. **121**, 6317 (2004).
[49] U. Even, J. Jortner, D. Noy, N. Lavie, and C. Cossart-Magos, J. Chem. Phys. **112**, 8068 (2000).
[50] E. Garand, T. I. Yacovitch, and D. M. Neumark, J. Chem. Phys. **130**, 064304 (2009).
[51] E. W. Hansen and P.-L. Law, J. Opt. Soc. Am. A **2**, 510 (1985).
[52] H. Köppel, W. Domcke, and L. S. Cederbaum, Adv. Chem. Phys. **57**, 59 (1984).
[53] E. Garand, K. Klein, J. F. Stanton, J. Zhou, T. I. Yacovitch, and D. M. Neumark, J. Phys. Chem. A **114**, 1374 (2010).
[54] J. Almlöf and P. R. Taylor, J. Chem. Phys. **86**, 4070 (1987).
[55] T. Ichino, A. J. Gianola, W. C. Lineberger, and J. F. Stanton, J. Chem. Phys. **125**, 084312 (2006).
[56] K. Klein, E. Garand, T. Ichino, D. M. Neumark, J. Gauss, and J. F. Stanton, Theor. Chem. Acc. **129**, 527 (2011).
[57] The wording "minimum energy C_{2v} geometry(ies)" found here and elsewhere in the manuscript is used in a precise sense: it refers to the geometry at which the minimum energy is found at a C_{2v} structure; it does not imply that such a structure is a minimum on the adiabatic potential energy surface.
[58] K. Raghavachari, G. W. Trucks, J. A. Pople, and M. Head-Gordon, Chem. Phys. Lett. **157**, 479 (1989).
[59] J. F. Stanton and R. J. Bartlett, J. Chem. Phys. **98**, 7029 (1993); A. I. Krylov, Annu. Rev. Phys. Chem. **59**, 433 (2008).
[60] K. Kowalski and P. Piecuch, J. Chem. Phys. **115**, 643 (2001); S. A. Kucharski, M. Włoch, M. Musiał, and R. J. Bartlett, J. Chem. Phys. **115**, 8263 (2001).
[61] While CCSD(T) has proven to be a very accurate (and affordable) treatment of electron correlation for "single reference" cases, a proper linear response approach for this method cannot be formulated. Hence, while we have used CCSD(T) for the $\tilde{X}^1A_1$ and the triplet states (all of which are the lowest states of their given symmetries, and described well by a single-reference approach), the more expensive EOMEE-CCSDT approach has been used for the excited singlet states. In determining the vertical energies V_0^I for these states, the EOMEE-CCSDT energies at the anion geometry are used, with respect to the full (and much more expensive to calculate) CCSDT energy of the anion. However, reoptimization of the anion was not performed. The energy differences are the EOMEE-CCSDT energies of the excited singlets relative to the CCSDT energy of the anion, but both calculations are done at the CCSD(T) anion geometry. Similarly, the normal coordinates used in the calculations are the CCSD(T) normal coordinates for the anion

in all cases. Differences between CCSD(T) and CCSDT properties of the anion are not significant and in no way compromise the results of this work.
[62]T. Ichino, J. Gauss, and J. F. Stanton, J. Chem. Phys. **130**, 174105 (2009).
[63]C. Lanczos, J. Res. Natl. Bur. Stand. **45**, 255 (1950).
[64]I. M. Mills, in *Molecular Spectroscopy: Modern Research*, edited by K. N. Rao and C. W. Mathews (Academic, New York, 1972), pp. 115–140.
[65]W. Schneider and W. Thiel, Chem. Phys. Lett. **157**, 367 (1989).
[66]J. F. Stanton, C. L. Lopreore, and J. Gauss, J. Chem. Phys. **108**, 7190 (1998).
[67]Term energies (T_e, in cm^{-1}) calculated with the ANO0 basis (using the ANO1 geometries) at the CCSDT and CCSDTQ levels of theory are: 10 372 and 10 470 ($\tilde{a}^3B_1$); 11 995 and 12 116 ($\tilde{b}^3A_2$); 20 173 and 20 298 ($\tilde{c}^3A_1$); 13 896 and 13 761 ($\tilde{A}^1A_2$); and 16 975 and 16 540 ($\tilde{B}^1B_1$). The corresponding corrections (CCSDTQ-CCSDT) of +98, +121, +126, −135, and −435 cm^{-1} have been applied to the (EOM-)CCSDT T_e values obtained with the larger ANO1 basis in the penultimate row of Table IV.
[68]cfour, coupled-cluster techniques for computational chemistry, a quantum-chemical program package by J. F. Stanton, J. Gauss, E. M. Harding, P. G. Szalay with contributions from A. A. Auer, R. J. Bartlett, U. Benedikt, C. Berger, D. E. Bernholdt, Y. J. Bomble, L. Cheng, O. Christiansen, M. Heckert, O. Heun, C. Huber, T.-C. Jagau, D. Jonsson, J. Jusélius, K. Klein, W. J. Lauderdale, D. A. Matthews, T. Metzroth, L. A. Mück, D. P. O'Neill, D. R. Price, E. Prochnow, C. Puzzarini, K. Ruud, F. Schiffmann, W. Schwalbach, S. Stopkowicz, A. Tajti, J. Vázquez, F. Wang, J. D. Watts, and the integral packages molecule (J. Almlöf and P. R. Taylor), props (P. R. Taylor), abacus (T. Helgaker, H. J. Aa. Jensen, P. Jørgensen, and J. Olsen), and ecp routines by A. V. Mitin and C. van Wüllen. For the current version, see http://www.cfour.de.
[69]M. Kállay and P. R. Surján, J. Chem. Phys. **115**, 2945 (2001).
[70]This is of course overly simplistic, as both q_2 and q_4 include some mixing with the "other" CC distance. A more complete picture is this: q_2 is an out-of-phase combination of the two CC stretches, with the outer C_2C_3 distance dominating; q_4 is in-phase, with the inner C_1C_2 distance playing the dominant role.
[71]A. M. Mebel, W. M. Jackson, A. H. H. Chang, and S. H. Lin, J. Am. Chem. Soc. **120**, 5751 (1998).
[72]B. Noller, M. Margraf, C. Schröter, T. Schultz, and I. Fischer, Phys. Chem. Chem. Phys. **11**, 5353 (2009).
[73]The prominence of both features—as well as the absence of the bending fundamental (ν_3) which would be between them—is easily explained by the geometry shifts that occur upon electron detachment from the anion (see Tables I and IV).
[74]The tail probably contains a minor contribution from a combination level, $\nu_2 + 2\nu_6$. The simulation, however, predicts this contribution to be much smaller than that from the $2\nu_5$ level. Also, the eBE for the $\nu_2 + 2\nu_6$ level is significantly higher than that for the $2\nu_5$ level.
[75]That the predicted ω_6 for the $\tilde{a}^3B_1$ state is very much in line with the other electronic states (see Table IV) also argues against strong coupling involving this mode in the present case. In addition, and providing further support for the assignment, there is a pronounced difference between ω_9 in the anion and the $\tilde{b}^3A_2$ state, which suggests that it should have reasonable Franck-Condon activity for even-quantum transitions in the $\tilde{a}^3B_1$ state.
[76]In this regard, there is some additional reproducible signal in the SEVI spectrum at an eBE near 25 600 cm^{-1} that could plausibly be assigned to $4\nu_9$. Although the magnitude of the anharmonicity here is substantial, its direction is consistent with vibronic coupling involving the higher-lying $\tilde{b}^3A_2$ state, and its magnitude is actually quite similar to that obtained in the model Hamiltonian calculations.
[77]It should be noted that both the $\nu_5 + \nu_6$ and $\nu_8 + \nu_9$ combination levels (both of which have overall a_1 vibrational symmetry) are expected to occur very near this region, and the possibility certainly exists that a Fermi resonance involving one or both of these combination levels and ν_4 causes the apparent splitting of this peak. The vibronic simulation—which reproduces this region of the spectrum quite well—predicts that the $\nu_8 + \nu_9$ combination level will have appreciable intensity and will also be located just below the stronger ν_4, just as observed. While modes q_5 and q_6 are not included in the simulations, this finding suggests that it is the $\nu_8 + \nu_9$ level that manifests itself in the fine structure of the SEVI spectrum and not $\nu_5 + \nu_6$. The absence of a $\nu_5 + \nu_6$ in the *simulated* spectrum is, of course, due to the fact that these modes were excluded from the simulations for the coupled triplet states. This was done because the harmonic frequencies of these two modes are quite similar in the anion, $\tilde{a}^3B_1$, and $\tilde{b}^3A_2$ triplet states. Nevertheless, a simulation was run that includes these modes, and essentially no intensity is observed for the combination level. Therefore, we are confident that $\nu_8 + \nu_9$ is the observed feature.
[78]The photodetachment cross section in the near-threshold region has been studied with a procedure similar to that employed by Brauman and coworkers (Ref. 88) as adopted by Krylov (Ref. 89). The Dyson orbitals for photodetachment to the A_2 and B_1 states were calculated with EOMIP-CCSD theory to evaluate the transition dipole matrix elements. Also, the plane wave function for the scattering electron was orthogonalized with the Dyson orbital as well as with those occupied anion molecular orbitals that have non-zero transition moment with the Dyson orbital. This model predicts significantly larger cross sections for detachment to the B_1 state than to the A_2 state in the near-threshold region.
[79]The stick spectrum and convoluted spectral profile make the assumption that the photodetachment cross sections for the two states are equal. However, when the results of the model calculation for the photodetachment cross section discussed in Ref. 78 are taken into account, agreement between the experiment and the spectral simulation improves.
[80]One piece of evidence that contributes to support the strong vibronic coupling between the $\tilde{a}^3B_1$ and $\tilde{b}^3A_2$ states that is clearly central to the analysis of this part of the spectrum is the near absence of the clearly Franck-Condon active q_2 mode (see Table IV) in the $\tilde{a}^3B_1$ state in the observed spectrum. From the *ab initio* calculations, one would expect to see ν_2 at an eBE near 26 800 cm^{-1}, which is in the general location of the "third" peak discussed in the main text. The stick spectrum suggests that the ν_2 level is heavily split by the vibronic interaction with its intensity spread out over a range of energy that "takes away" what would otherwise be a conspicuous peak.
[81]While the peak at eBE = 28 160 cm^{-1} is in (nearly) the right place to be associated with ν_2 of the $\tilde{b}^3A_2$ state, the position is nevertheless about 100 cm^{-1} above where the ν_2 level would be expected based on the *ab initio* calculations. Moreover, the simulation of the photodetachment spectrum for the excited singlet final states shows that the $\tilde{A}^1A_2$ origin is expected to be strong, which is consistent with this assignment rather than the ν_2 fundamental of the $\tilde{b}^3A_2$ state.
[82]That is, the geometry difference in q_2 is smaller between the anion and the $\tilde{B}^1B_1$ state than between the $\tilde{X}^1A_1$ and $\tilde{B}^1B_1$ states.
[83]The empirical shift of the gap between the $\tilde{A}^1A_2$ and $\tilde{B}^1B_1$ states was made so that the "ν_2" band becomes coincident with the experimental feature. In addition, the direction of the shift is consistent with the correction arising from quadruple excitations (see Table IV), the magnitudes being 800 (empirical shift) and 300 cm^{-1} (CCSDTQ-CCSDT), respectively. Note that the effect of basis set (see Table IV and Ref. 67) is greater for the $\tilde{B}^1B_1$ state, so that one expects further augmentation to narrow the gap yet more. To further address this issue, energies of the $\tilde{A}^1A_2$ and $\tilde{B}^1B_1$ states were calculated at the CCSD level of theory with the cc-pVQZ and cc-pV5Z basis sets, and then extrapolated to the basis set limit. The difference between this extrapolated limit (at the CCSD level) and the corresponding ANO1 calculation (all of these values correspond to the frozen-core approximation) is −266 cm^{-1}. Finally, the effect of the frozen-core treatment was investigated by calculating frozen-core and all-electron energies using the cc-pCVTZ basis set; this found that the all-electron gap between the $\tilde{A}^1A_2$ and $\tilde{B}^1B_1$ states is 60 cm^{-1} lower than the frozen core value. Taken together, the ANO1/CCSDT vertical gap of 3573 cm^{-1} between the $\tilde{A}^1A_2$ and $\tilde{B}^1B_1$ states should be reduced by 626 (=300 + 266 + 60) cm^{-1}, a magnitude that is broadly consistent with that applied to the Hamiltonian to best reproduce the experimental spectrum in this region.
[84]Of course, the smallest member of this series is vinylidene ($H_2C{=}C{:}$), but this species isomerizes to acetylene on a picosecond time scale [see K. M. Ervin, J. Ho, and W. C. Lineberger, J. Chem. Phys. **91**, 5974 (1989)] and is consequently not a realistic candidate for interstellar observation.
[85]A. E. Douglas, Nature (London) **269**, 130 (1977).
[86]M. L. Heger, Lick Obs. Bull. **10**, 146 (1922); T. P. Snow and B. J. McCall, Astron. Radioastron. Astrophys. **44**, 367 (2006); P. J. Sarre, J. Mol. Spectrosc. **238**, 1 (2006).
[87]H. Linnartz, N. Wehres, H. Van Winckel, G. A.H. Walker, D. A. Bohlender, A. G. G. M. Tielens, T. Motylewski, and J. P. Maier, Astron. Astrophys. **511**, L3 (2010).
[88]K. J. Reed, A. H. Zimmerman, H. C. Andersen, and J. I. Brauman, J. Chem. Phys. **64**, 1368 (1976).
[89]C. M. Oana and A. I. Krylov, J. Chem. Phys. **131**, 124114 (2009).